

Fiscal Year 2023 Filtration of Hanford Tank 241-SY- 101 Supernatant at 16 °C

August 2023

JR Allred
C Alvarez
EC Buck
CA Burns
RC Daniel
JGH Geeting
AM Westesen
RA Peterson

DISCLAIMER

This report was prepared as an account of work sponsored by an agency of the United States Government. Neither the United States Government nor any agency thereof, nor Battelle Memorial Institute, nor any of their employees, makes **any warranty, express or implied, or assumes any legal liability or responsibility for the accuracy, completeness, or usefulness of any information, apparatus, product, or process disclosed, or represents that its use would not infringe privately owned rights.** Reference herein to any specific commercial product, process, or service by trade name, trademark, manufacturer, or otherwise does not necessarily constitute or imply its endorsement, recommendation, or favoring by the United States Government or any agency thereof, or Battelle Memorial Institute. The views and opinions of authors expressed herein do not necessarily state or reflect those of the United States Government or any agency thereof.

PACIFIC NORTHWEST NATIONAL LABORATORY
operated by
BATTELLE
for the
UNITED STATES DEPARTMENT OF ENERGY
under Contract DE-AC05-76RL01830

Printed in the United States of America

Available to DOE and DOE contractors from the
Office of Scientific and Technical Information,
P.O. Box 62, Oak Ridge, TN 37831-0062;
ph: (865) 576-8401
fax: (865) 576-5728
email: reports@adonis.osti.gov

Available to the public from the National Technical Information Service
5301 Shawnee Rd., Alexandria, VA 22312
ph: (800) 553-NTIS (6847)
email: orders@ntis.gov <<https://www.ntis.gov/about>>
Online ordering: <http://www.ntis.gov>

Fiscal Year 2023 Filtration of Hanford Tank 241-SY-101 Supernatant at 16 °C

August 2023

JR Allred
C Alvarez
EC Buck
CA Burns
RC Daniel
JGH Geeting
AM Westesen
RA Peterson

Prepared for
the U.S. Department of Energy
under Contract DE-AC05-76RL01830

Pacific Northwest National Laboratory
Richland, Washington 99354

Summary

Approximately 9 liters of supernatant from Hanford waste tank 241-SY-101 was delivered by Washington River Protection Solutions to the Radiochemical Processing Laboratory (RPL) at Pacific Northwest National Laboratory. The thirty-six SY-101 sample bottles consisted of six sets of six samples, with each set pulled from a unique tank sampling level. Prior to testing, samples from each level were composited to provide nominally level-independent feed for dead end filtration and ion exchange testing.

The composited 241-SY-101 supernatant was chilled to 16 °C for 1 week prior to testing. Filtration testing was then conducted using a backpulse dead-end filter (BDEF) system equipped with a feed vessel and a Mott inline filter Model 6610 (Media Grade 5) in the hot cells of the RPL. This was done to provide waste processing benchmarks for 200 West Area wastes in the West Area Risk Management project.

The feed was filtered through the BDEF system at a targeted flux of 0.065 gpm/ft². During filtration the differential pressure required to effect filtration at 0.065 gpm/ft² increased little over the filtration campaign and never reached 2 psid (the Tank Side Cesium Removal system action limit). This indicates that the Media Grade 5 filter should perform well when processing SY-101 supernatant. After completing filtration of the SY-101 feed, the filter was cleaned.

Solids concentrated from the backpulse solutions displayed calcium phosphate, aluminum oxides, and aluminum-chromium nanoparticle agglomerates. Electron diffraction was used to determine the types of phases that were present in the solids. Most of the phases found were only weakly crystalline. The identifications of the phases therefore are tentative.

Acknowledgments

The authors gratefully acknowledge the help of hot cell technicians Victor Aguilar and Robert Cox in conducting this work. We thank Renee Russell for conducting the technical review of this report. We also thank Matt Wilburn for technical editing of this report and David MacPherson for the quality reviews of the calculation packages and this report.

Microscopy work was performed at the Radiochemical Processing Laboratory Quiet-Suite at Pacific Northwest National Laboratory.

Acronyms and Abbreviations

AEA	alpha energy analysis
BDEF	backpulse dead-end filter (system)
CWF	clean water flux
DEF	dead-end filtration
EDS	X-ray energy dispersive spectroscopy
HAADF	high-angle annular dark-field
HRTEM	high-resolution transmission electron microscopy
ICP-OES	inductively coupled plasma optical emission spectroscopy
IX	ion exchange
LAW	low-activity waste
MFC	mass flow controller
PNNL	Pacific Northwest National Laboratory
QA	quality assurance
R&D	research and development
RPL	Radiochemical Processing Laboratory
SAED	selected area electron diffraction
SEM	scanning electron microscopy
STEM	scanning transmission electron microscopy
TEM	transmission electron microscopy
TMP	transmembrane pressure
TRU	transuranic
TSCR	Tank Side Cesium Removal
WRPS	Washington River Protection Solutions
WTP	Waste Treatment and Immobilization Plant
WWFTP	WRPS Waste Form Testing Program

Contents

Summary	ii
Acknowledgments.....	iii
Acronyms and Abbreviations	iv
Contents	v
1.0 Introduction.....	1.1
2.0 Quality Assurance.....	2.1
3.0 Test Conditions	3.1
3.1 BDEF Filtration	3.1
3.1.1 Backpulse Dead-End Filter System Description	3.1
3.1.2 System Operation during Testing.....	3.3
3.2 Feed Composite	3.4
3.3 Feed Temperature Control.....	3.5
3.4 Sample Analysis	3.6
4.0 Results.....	4.1
4.1 Compositing Process Results.....	4.1
4.2 Stability Study Results.....	4.1
4.3 Clean Water Flux	4.3
4.4 Waste Filtering.....	4.4
4.5 Final CWF.....	4.10
4.6 Analytical Results.....	4.11
4.6.1 Compositing SY-101 Supernate Tank Waste Analysis	4.11
4.6.2 Total Alpha Energy Analysis	4.11
4.6.3 Rheology Analysis of Filtered and Cesium Decontaminated SY-101 Supernate Tank Waste	4.12
4.7 Microscopy Solids Analysis	4.12
5.0 Conclusions.....	5.1
6.0 References.....	6.1
Appendix A – BDEF Piping and Instrumentation Diagram	A.1
Appendix B – Feed Bottle Composite	B.1
Appendix C – Total Alpha Analysis for Filtration Permeate Samples	C.1
Appendix D – ICP-OES Analysis for As-Received 241-SY-101 Supernatant.....	D.1
Appendix E – Backpulsed Solids from SY-101 Characterization with Scanning Transmission Electron Microscopy.....	E.1

Figures

Figure 3.1.	BDEF system installed in hot cell. HTX = heat exchanger.	3.1
Figure 3.2.	(a) Filter housing schematic (note that the 6610 series filter was welded to a 3/8-in. pipe fitting, making the configuration similar to the 6480 series illustrated here); (b) photo of modified filters with filter housings removed. (Mott 6480 line filter schematic from https://mottcorp.com .)	3.2
Figure 3.3.	SY-101 temperature in the trough heat exchanger.....	3.5
Figure 3.4.	SY-101 temperatures in the BDEF recirculation loop (TE-101) and clamshell (TE-102, TE-103).	3.6
Figure 3.5.	Concentrated solids after centrifuging in hot cell.	3.7
Figure 3.6.	Concentrated solids in fumehood after centrifuging.	3.8
Figure 4.1.	Stability study sample after 1 week.	4.1
Figure 4.2.	Stability study sample after 1 week, sluiced via pipette.	4.2
Figure 4.3.	Stability study sample after 2 weeks.	4.2
Figure 4.4.	Reference stability study sample (left at ambient cell temperature, 23-24 °C, after 2 weeks, sluiced via pipette).	4.3
Figure 4.5.	Stability study sample temperature.	4.3
Figure 4.6.	CWF measurements for Media Grade 5 BDEF at 2.57 mL/min (0.065 gpm/ft ²) permeate rate (nominal) before testing. (Dashed line is average pressure over the 10-minute period.).....	4.4
Figure 4.7.	Filter differential pressure and MFC flow rate during filtering operations.....	4.6
Figure 4.8.	SY-101 filter resistance and permeate density during filtration process.....	4.7
Figure 4.9.	Fit to initial fouling experimental data using classical fouling mechanisms.....	4.9
Figure 4.10.	Fit to fouling prior to backpulse 1 experimental data using classical fouling mechanisms.	4.9
Figure 4.11.	Initial and final clean water flux.	4.10
Figure 4.12.	(A-D) SEM images of SY-101 solids showing a variety of morphologies and agglomerates, in some instances, >200 μm in diameter.....	4.13
Figure 4.13.	(A) Medium magnification STEM image and (B) TEM image of the same region (indicated by the red arrow) showing regions where SAED were collected (orange circles and shown in Figure D.2), and (C) STEM-EDS maps showing the occurrence of aluminum oxide, chromium-bearing phase, iron particle, and calcium phosphate phase.	4.14
Figure 4.14.	(A) Electron diffraction of Al-phase matched to boehmite, (B) electron diffraction pattern of apatite, (C) TEM image of a nano-structured material revealed with indicated regions where SAED were obtained, (D) STEM-HAADF of the same region, (E) high-resolution TEM of Al-phase indicating crystallinity (see insert FFT), and STEM-EDS maps of O, Al, P, Ca, Cr, and Fe.	4.15
Figure 4.15.	SEM image using a STEM detector showing different morphologies of particles from the SY-101 sample. Analysis excluded the very large particles shown in Figure 4.9.	4.16

Tables

Table 3.1.	Mass balance – BDEF.....	3.4
Table 3.2.	As-received samples.....	3.4
Table 4.1.	System timeline.....	4.5
Table 4.2.	Test parameters prior to backpulsing.....	4.6
Table 4.3.	Filtration regime exponent n and blocking parameter σ	4.8
Table 4.4.	Post filtration density measurements of product bottles.	4.10
Table 4.5.	ICP-OES results of composited SY-101 supernate tank waste.....	4.11
Table 4.6.	AEA for permeate samples.	4.11
Table 4.7.	Viscosity results of filtered and Cs decontaminated sample.....	4.12
Table 4.8.	Compositional analysis of Cr-bearing Al-phase.	4.15
Table 4.9.	Electron diffraction from Cr-bearing Al-phase.....	4.16

1.0 Introduction

The U.S. Department of Energy's Hanford Site houses 56 million gallons of highly radioactive tank waste generated from plutonium production from 1944 to 1988 (Gerber 1992). The supernatant waste, currently stored in underground tanks, is intended to be vitrified following filtration and ^{137}Cs removal at the Waste Treatment and Immobilization Plant (WTP) Pretreatment Facility. Because the WTP Pretreatment Facility is not currently operational, ^{137}Cs will be removed from low-activity waste (LAW) vitrification feeds using the Tank Side Cesium Removal (TSCR) system in a technology demonstration that will filter and then remove cesium from tank waste supernate to support transferring the TSCR-processed waste directly to the WTP LAW Facility. The TSCR system is skid-mounted and employs two key technologies: (1) dead-end filtration (DEF) for solids removal, which is necessary to protect the functionality of the ion exchange (IX) columns, and (2) IX for cesium removal.

A small-scale test platform was established in 2017 to demonstrate these processes in the Pacific Northwest National Laboratory (PNNL) 325 Building, also known as the Radiochemical Processing Laboratory (RPL).

Previous PNNL test platform campaigns have focused on wastes from the Hanford 200 East Area. The primary objective of activities covered in this testing is to provide waste processing benchmarks for 200 West Area wastes in the West Area Risk Management project. The first 200 West Area waste considered for testing is waste from tank 241-SY-101 (hereafter shortened to "SY-101"). For SY-101 supernatant, the testing aims to (a) demonstrate DEF of an actual waste feed at reduced temperature to obtain prototypic TSCR flux rates and identify issues that may impact filtration and (b) provide feed for the IX unit operation (also part of the test platform). Approximately 9 liters of SY-101 tank waste supernatant was delivered to PNNL in thirty-six 250-mL bottles. The thirty-six SY-101 sample bottles consisted of six sets of six samples, with each set pulled from a unique tank sampling level. Prior to testing, samples from each level were composited to provide nominally level-independent feed for DEF and IX testing.

The SY-101 tank waste was filtered at reduced temperature (16 °C) to mimic the low end of temperatures that tank 241-SY-101 can experience during the winter and spring months. Note that the SY-101 sample feed temperature was not controlled after the feed samples were collected from the tank by Washington River Protection Solutions (WRPS) and stored at the PNNL hot cell ambient temperature (~25 °C) from delivery until approximately 1 week prior to filtration at PNNL. The sodium content of the as-received SY-101 samples was expected to range from 2.8 to 4.0 M (Detrich 2019), and as such, SY-101 level-composites were not diluted with Columbia River water to reduce their sodium molarity as has been done in previous DEF and IX test campaigns (e.g., see Allred et al. 2022).

The current filtration testing was conducted using a purpose-built filtration system, called the backpulse dead-end filter (BDEF) system, which was designed to mimic planned filtration to be used in the full-scale TSCR system. This equipment was used in fiscal years (FYs) 20 and 21 and is described in Allred et al. (2020). It was also used under current fiscal year filter testing of Hanford tank 241-AP-105 waste [see TP-DFTP-134, Rev. 0.0 (Geeting 2022), not commercially available].

2.0 Quality Assurance

All research and development (R&D) work at PNNL is performed in accordance with PNNL's Laboratory-Level Quality Management Program, which is based on a graded application of NQA-1-2000, *Quality Assurance Requirements for Nuclear Facility Applications* (ASME 2000), to R&D activities. To ensure that all client quality assurance (QA) expectations were addressed, the QA controls of PNNL's WRPS Waste Form Testing Program (WWFTP) QA program were also implemented for this work. The WWFTP QA program implements the requirements of NQA-1-2008, *Quality Assurance Requirements for Nuclear Facility Applications* (ASME 2008), and NQA-1a-2009, *Addenda to ASME NQA-1-2008* (ASME 2009).

The work described in this report was assigned the technology level "Applied Research." All staff members contributing to the work received proper technical and QA training prior to performing quality-affecting work.

3.0 Test Conditions

In November 2022, WRPS collected 36 supernatant samples (~250 mL each) from tank SY-101 in two batches. These samples were taken at six depths (26, 81, 135, 187, 240, and 294 in. below the liquid surface level¹) in groups of six and provided to PNNL for filtration testing. At the RPL, the as-received SY-101 samples from each level were composited to provide nominally level-independent feed for filtration and IX. The bottles of composited SY-101 tank waste were chilled (16 °C setpoint) for approximately 1 week prior to testing. Filtration testing of the tank waste used a Mott Model 6610 (Media Grade 5) sintered 316L stainless steel line filter with a 0.317-in. porous diameter, 1.463-in. porous length, and 1.51-in.² filter area with porous end cap. Filtration testing of the SY-101 tank waste began on March 19, 2023.

3.1 BDEF Filtration

3.1.1 Backpulse Dead-End Filter System Description

The filtration system is the same system that was used in FY22 (Allred et al. 2022), again using the trough heat exchanger to keep all the feed at the setpoint temperature until it was added to the BDEF system. The feed bottles were stored in the trough heat exchanger with a cover until the feed was transferred to the BDEF system.

Once the feed was added to the BDEF, the existing heat exchanger kept the feed at the setpoint temperature in the reservoir and in the BDEF recirculation loop. The filter housing clamshell heat exchanger kept the feed at the setpoint temperature as it exited the recirculation loop until it was filtered. After filtration, the temperature was no longer controlled. A piping and instrumentation diagram is provided in Appendix A. Figure 3.1 shows a photograph of the BDEF system installed in the RPL Shielded Analytical Laboratory hot cell.

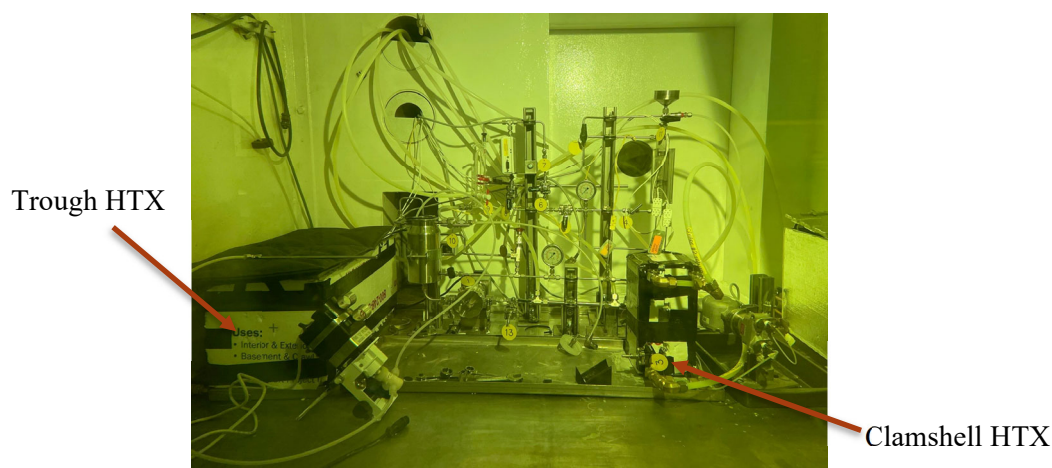


Figure 3.1. BDEF system installed in hot cell. HTX = heat exchanger.

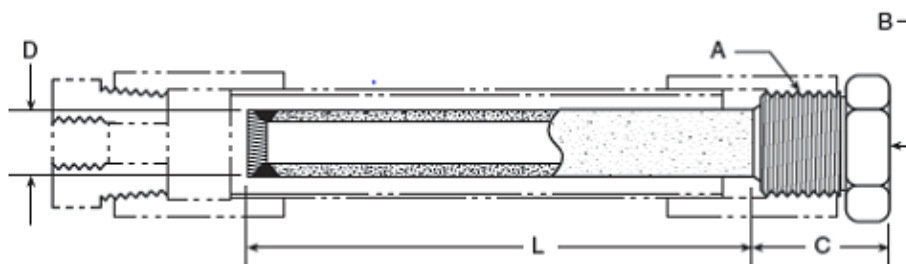
¹ Per RPP-PLAN-65336, *Tank 241-SY-101 Large Volume Sample Collection to Support Platform Testing, Phase 1, FY23*, and RPP-PLAN-65337, *Tank 241-SY-101 Large Volume Sample Collection to Support Platform Testing, Phase 2, FY23*.

The BDEF system is composed of a slurry recirculation loop, a filter assembly, and a permeate system. The main recirculation loop consists of a 1-liter stainless steel container (Eagle, EPV1A), a low-shear quaternary diaphragm pump (Quattro Flow QF150), a heat exchanger, and a throttle valve. The pump speed is controlled by a variable frequency drive that is located outside the hot cell. The slurry flow rate and pressure are controlled by adjusting the pump variable frequency drive (pump speed control) and throttle valve. The recirculation loop provides mixed, pressurized feed to the filter assembly. During the testing described in this report, the slurry temperature was controlled at a 16 °C setpoint.

The filter assembly receives pressurized slurry from the slurry recirculation loop. The filter assembly is composed of a filter, a Rosemount differential pressure transducer, and a flush valve (V3 in Appendix A). The flush valve is actuated during backpulse operations used to clear solids off the filter and out of the system.

The permeate system receives permeate produced by the filter assembly. The permeate flow rate is controlled with a mass flow controller (MFC), which can control feed in the range of 0.15 to 0.33 L/hour. (These rates equate to allowable filter areas of 1.5 to 3.3 in.² assuming flux of 0.065 gpm/ft².) The MFC measures flow rate and density of the permeate, and a glass flowmeter is provided as a secondary flow rate measurement device. The permeate system can also perform a backpulse function. Pressurized air can be introduced into the backpulse chamber and used to force permeate (or other fluids) backward through the filter and out of the system.

The Mott 6610 filter used in testing is cylindrical, with dimensions of 0.317-in. diameter × 1.5-in. length and a filtration area of 1.51 in.². The filter element is fabricated from a seamless sintered stainless-steel tube that is a closed/dead-end porous tube (with a porous end cap); the open end is welded to a pipe-reducing bushing. At 0.065 gpm/ft², the rate of filter processing is 3.7 L of feed per 24-hour day. Figure 3.2 shows a schematic of the filter assembly and a photo of the filter.



(a)



(b)

Figure 3.2. (a) Filter housing schematic (note that the 6610 series filter was welded to a 3/8-in. pipe fitting, making the configuration similar to the 6480 series illustrated here); (b) photo of modified filters with filter housings removed. (Mott 6480 line filter schematic from <https://mottcorp.com>.)

3.1.2 System Operation during Testing

The steps used to test the SY-101 waste samples are outlined below.

1. Composite of SY-101 feed: Six sets of ~1.5 L of waste were collected from six unique sampling depths in tank SY-101. Based on current SY-101 physical and chemical properties (Detrich 2019), it was expected that DEF- and IX-relevant physical properties (e.g., viscosity and sodium molarity) would vary as a function of sampling depth. To provide level-independent feed for DEF and IX testing, samples from each set were composited with each other to minimize set-to-set variation in physical/chemical properties. First, 200 mL of waste was sampled from each of the six sampling level sets and consolidated into a single 1.2-L feed bottle. This process was repeated five additional times to create a total of six 1.2-L level-composited feed bottles for testing. The remaining 300 mL of waste in each of the six level-sets (1.8 L total) was composited into a single “heel” 2-L bottle. A fraction of the original or composited feed was set aside and its stability with respect to precipitation studied (see note below).

Note: During the compositing process, an approximately 250 mL sample of SY-101 feed was set aside from the primary feed composites, chilled to 16 °C, and held at that temperature for at least 2 weeks, during which time it was monitored for precipitation of solids (in particular, $\text{Na}_3\text{PO}_4 \cdot 12\text{H}_2\text{O}$ solids).

2. Temperature control of SY-101 prior to filtration: Approximately 1 week prior to filtration, the composited SY-101 feeds were chilled to 16 °C and held for approximately 1 week at the reduced temperature.
3. Clean water flux (CWF) measurement: The CWF measurement served as a system leak test and provided a baseline measurement of the filter resistance and was conducted at nominal test conditions of 0.065 gpm/ft² and run for approximately 10 minutes.
4. Filtration of the SY-101 composited waste: Filtration was performed using a Mott Grade 5 sintered metal filter at a targeted flux of 0.065 gpm/ft². The targeted flux was based on the scaled flux used during AVANTech testing¹ (0.306 gpm through 4.7 ft² of Mott sintered metal filter [0.065 gpm/ft²]). Filtration was performed at a targeted temperature of 16 °C. Filter resistance as a function of time was measured and the filter was backflushed (“backpulsed”) if the differential pressure increased to 2 psi across the filter. Backflush solutions were collected and, if solids were found, they were analyzed.
5. Filter cleaning: The filter was cleaned using a prototypic TSCR protocol by soaking in 0.1 M NaOH for a minimum of 2 hours.
6. Filtered permeate from testing was collected and retained for use as feed for subsequent IX testing. Temperature control (to 16 °C) of the filtered samples was maintained to the best extent practicable, such that filtered permeates were returned to the trough after collection in any given bottle was complete.
7. CWF: After cleaning, the BDEF was rinsed and another CWF test was executed on the filter.
8. The BDEF system was laid-up for storage.

Table 3.1 provides a mass balance for BDEF testing. A total of 9,677.5 g of SY-101 supernatant was added to the BDEF system during testing, and a total of 9,560.9 g was removed. The missing mass (~116.6 g) is due to evaporation and material that wets the inside of the BDEF system. It is not recoverable and represents less than 1.2% of the initial feed.

Table 3.1. Mass balance – BDEF.

Description	In (g)	Out (g)
Decanted supernate filtration	9,677.5	
Product to IX		9,441.8
Permeate samples		13.4
Backpulse samples		76.5
Drained from BDEF		29.2
Total	9,677.5	9,560.9

3.2 Feed Composite

Tank waste supernate was sampled from six unique liquid levels of tank 241-SY-101, with six 250-mL bottles received from each sample level for a total of 36 bottles. The samples were taken from tank liquid depths of 26, 81, 135, 187, 240, and 294 in. as shown in Table 3.2. Liquid properties such as viscosity, sodium molarity, and density can vary based on depth beneath the liquid surface due to stratification. A density measurement was taken from one bottle of each sampled depth prior to the compositing process. Two-hundred mL of a receipt bottle from each sampling location was combined into single 1.5-L filtration feed bottles for nominally 1,200 mL of composited waste in each feed bottle. The heels of each of the receipt bottles were subsequently composited in 1.5-L feed bottles by combining two receipt bottles heels from each level into single feed bottles. Composited bottle composition details can be found in Appendix B.

Table 3.2. As-received samples.

Sample Location (depth below liquid surface, in.)	Receipt Sample Bottle ID		Density (g/mL)
26	SY-23-01	SY-23-02	1.13402
	SY-23-03	SY-23-04	
	SY-23-05	SY-23-06	
	SY-23-07	SY-23-08	
81	SY-23-09	SY-23-10	1.13326
	SY-23-11	SY-23-12	
	SY-23-13	SY-23-14	
135	SY-23-15	SY-23-16	1.13548
	SY-23-17	SY-23-18	
	SY-23-19	SY-23-20	
187	SY-23-21	SY-23-22	1.13508
	SY-23-23	SY-23-24	
	SY-23-25	SY-23-26	
240	SY-23-27	SY-23-28	1.13458
	SY-23-29	SY-23-30	
	SY-23-31	SY-23-32	
294	SY-23-33	SY-23-34	1.15586
	SY-23-35	SY-23-36	

3.3 Feed Temperature Control

Figure 3.3 shows the temperature profile of the chilled SY-101 filtration feed prior to entering the BDEF system. The feed was held at a 16 °C setpoint temperature beginning on 1/19/2023 – 13 days leading up to the filtration test – and continued to be maintained at that setpoint throughout the filtration process. A 100-ohm platinum resistance temperature detector probe (TE-104) was submerged into a feed bottle in the trough heat exchanger to measure feed temperature throughout the chilling. TE-104 was held in place using a lid with a feedthrough fastened to a feed bottle to allow TE-104 to be submerged while mitigating spill risk.

The feed trough temperature was maintained within the range of 16 °C ± 2.2 °C throughout filtration with the exception of three spikes in 5-minute average temperatures reported by TE-104. The first spike was an increase to 18.8 °C on 3/20/2023 at 1430 during normal filtration operation and the second spike was an increase to 18.8 °C on 3/21/2023 at 0541. Due to the impulse nature of these temperature increases followed by the immediate return to nominal operating temperatures, it is likely these two reported temperatures are not reflective of the actual feed bottle temperature. The third spike in temperature to reach outside the 16 °C ± 2.2 °C range was a drop to 13.7 °C occurring on 3/21/23 at 1746. This impulse followed the removal of TE-104 from the final feed bottle and therefore was not an accurate measurement of the remaining feed solution.

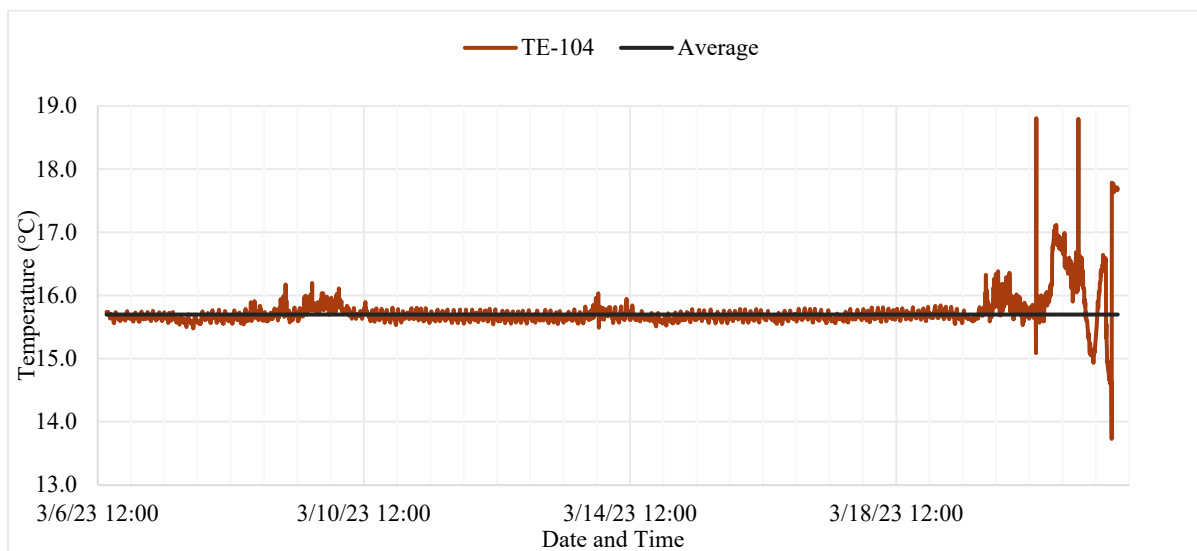


Figure 3.3. SY-101 temperature in the trough heat exchanger.

The temperature of the SY-101 slurry in the BDEF recirculation loop as reported by TE-101 throughout testing is shown in Figure 3.4. Overlain in the same figure are the slurry stream temperatures immediately upstream (TE-102) and downstream (TE-103) of the filter, thermocouples measuring these temperatures were contained within the clamshell heat exchanger. There is a simultaneous gradual reduction in temperature reported by TE-102 and TE-103 of ~2.5 °C from 03/19/23 at approximately 2130 until 3/20/23 at approximately 1900 while TE-101 showed a smaller decrease of ~0.5 °C during the same period. While the exact cause of this temperature reduction is unknown, all three reported temperatures remained within the 16 °C ± 2.2 °C threshold during this period. A spike in offset of ~2 °C between TE-102 and TE-103 temperatures was observed on 3/21/2023 at 1531 while both temperatures remained within the acceptable temperature range. Significant temperature deviations in both TE-102 and TE-103 began on 3/21/2023 at 1856. This was following the initial reduction in pump speed at 1732, with continuous reduction in pump speeds occurring through the end of filtration at 1950.

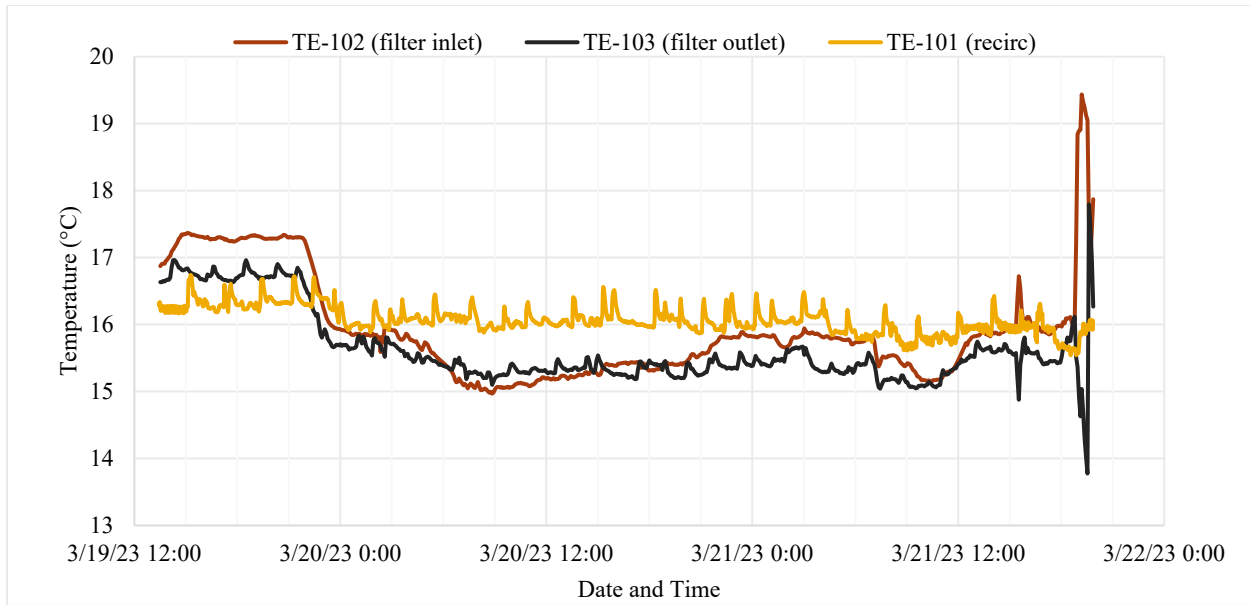


Figure 3.4. SY-101 temperatures in the BDEF recirculation loop (TE-101) and clamshell (TE-102, TE-103).

3.4 Sample Analysis

Three permeate samples were collected (TI-145-P1, TI-145-P2, TI-145-P3) after approximately 1/3, 2/3, and 3/3 of the SY-101 feed had been filtered. These samples were submitted for total alpha analysis to determine the transuranic (TRU) content of the filtered permeate.

Backpulse concentrates were retained and kept separate. Upon completion of filtration testing, the solids were concentrated as shown in Figure 3.5. To concentrate solids, solution collected was centrifuged at 2,500 rpm for 15 minutes. The bulk amount of the supernatant was decanted and the solids from the centrifuge tubes were suspended and combined. The concentrated solution was again centrifuged at 2,500 rpm for 15 minutes. More supernatant was removed, the solids suspended, and transferred out of the hot cell. Once removed from the hot cell, the concentrated solution was transferred to the smaller 15-mL centrifuge tube and the solids spun down for 2 minutes at 3,000 rpm. Additional supernatant was removed to reduce the dose of the sample prior to sending it to the microscopy staff. Figure 3.6 shows the solids that were collected from the backpulsed solution after centrifuge and decant iterations.

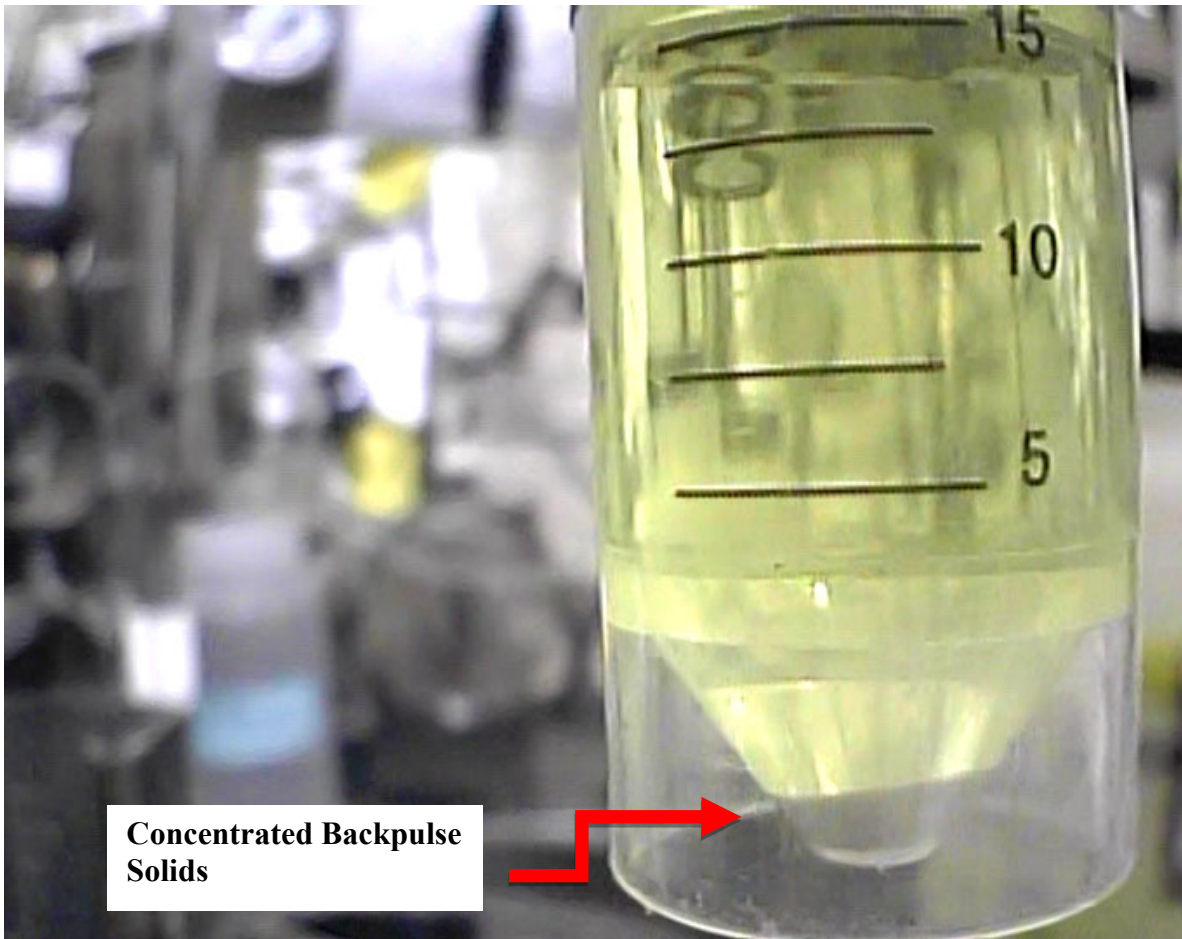


Figure 3.5. Concentrated solids after centrifuging in hot cell.



Figure 3.6. Concentrated solids in fumehood after centrifuging.

4.0 Results

4.1 Compositing Process Results

A sample from the composited bottle BDEF-SY1-1 was checked for density. Density was measured using a 10-mL Class A volumetric flask and an analytical balance. For batch 1, density was measured to be 1.126 g/mL at an ambient cell temperature of 24.5 °C. The Na concentration was not measured after compositing but was measured after filtration (which should not affect Na concentration) and will be included in the IX report for FY23 (RPT-DFTP-040, *Reduced Temperature Cesium Removal from SY-101 Using Crystalline Silicotitanate*; currently being drafted).

4.2 Stability Study Results

A 200-mL subsample from composited bottle BDEF-SY1-6 was added back to a relabeled 250-mL receipt bottle. A reference subsample (5 mL) of the same solution was placed in a 20-mL centrifuge tube and left at ambient cell temperature for the duration of the stability study. The 200-mL subsample was placed in the cooling trough set to 16 °C on 2/9/2023. On 2/16/2023, the sample was pulled from the cooling trough for observation. Figure 4.1 displays the bottle bottom highlighting a thin layer of solids. To better characterize these solids, a pipette was used to sluice the bottom of the bottle and agitate these solids as shown in Figure 4.2. The solids were found to be small, white, and easily dispersed. Once observation was complete, the sample was placed back in the cooling trough and cooled for another week. On 2/23/2023, the sample was pulled again and observed, see Figure 4.3. The sample appeared to be largely unchanged. Close inspection may suggest a slightly thicker layer of solids on the bottom of the jar. A pipette was again used to sluice the bottom of the bottle and agitate these solids, with the solids showing the same behavior as in week 1. The reference subsample was observed at week 2, and the same thin layer of solids was observed; it was also agitated via pipette, shown in Figure 4.4. No large crystals of sodium phosphate were observed in either sample. Figure 4.5 provides the recorded temperature of the thermostating de-ionized water bottle in the cooling trough.

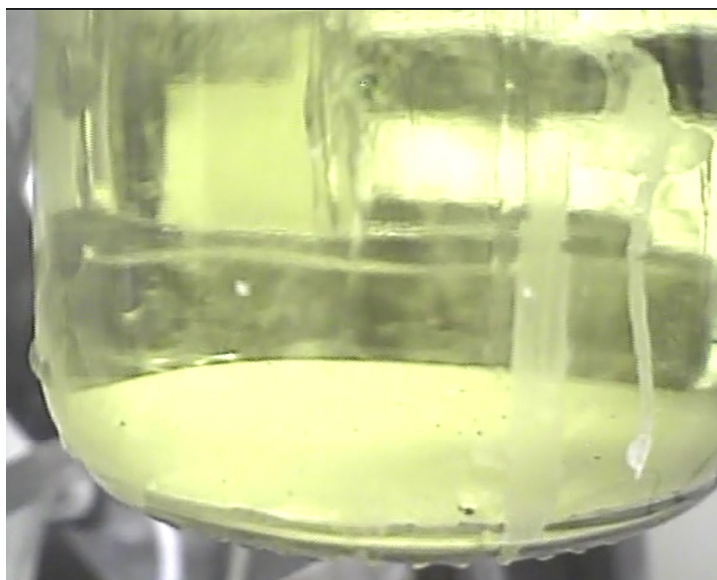


Figure 4.1. Stability study sample after 1 week.



Figure 4.2. Stability study sample after 1 week, sluiced via pipette.

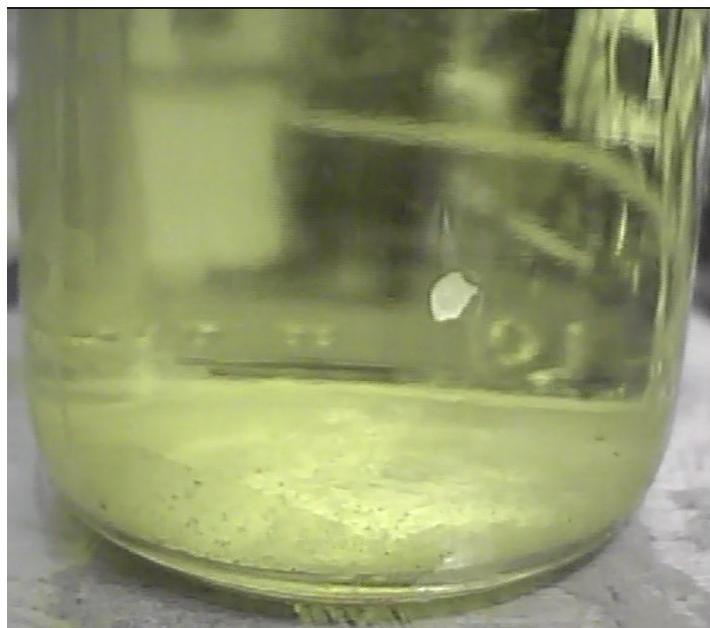


Figure 4.3. Stability study sample after 2 weeks.

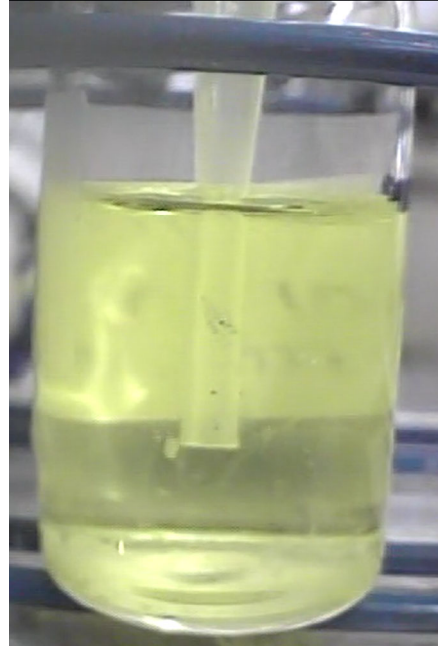


Figure 4.4. Reference stability study sample (left at ambient cell temperature, 23-24 °C, after 2 weeks, sluiced via pipette).

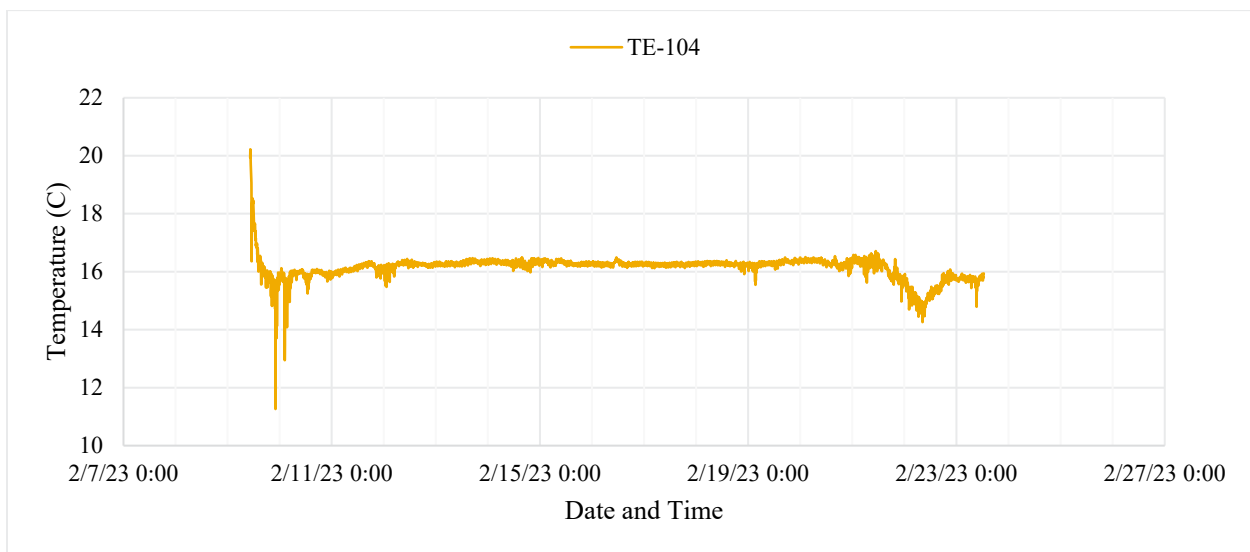


Figure 4.5. Stability study sample temperature.

4.3 Clean Water Flux

The objective of the CWF was to assess the state of the system at the start of testing to ensure a uniform basis for comparing different filtration trials, and in particular to ensure that the system was “clean” at the start of testing. Figure 4.6 shows the initial CWF at 15.9 °C using 0.01 M NaOH with the Media Grade 5 stainless steel BDEF filter. The CWF tests were conducted at ambient cell temperature at a nominal 2.57 mL/min (0.065 gpm/ft²) permeate flow rate. The transmembrane pressure (TMP) averaged 0.116 psid in the initial CWF with an average filter resistance of $1.65 \times 10^{10} \text{ m}^{-1}$. Resistance, $R \text{ [m}^{-1}\text{]}$, is calculated via Darcy’s law:

$$Q = \frac{PA_t}{\mu R} \quad (4.1)$$

where Q is the volumetric flow rate [m^3/s], P is the TMP [Pa], A_t is the total filter area [m^2] [$9.74 \times 10^{-4} \text{ m}^2$], and μ is the filtrate dynamic viscosity [$\text{Pa}\cdot\text{s}$] (assumed to be 1.111 cP at 15.9 °C). Rearranging so that:

$$R(t) = \frac{P(t)A_t}{\mu Q(t)} \quad (4.2)$$

Prior CWF results on the BDEF system with this filter ranged from 0.015 to 0.2 psid TMP (Allred et al. 2022). These values all are likely within the accuracy of the CWF measurement and represent a relatively clean filter. Estimates of the resistance for the Mott 6610 series Grade 5 are on the order of $2 \times 10^{10} \text{ m}^{-1}$. The average TMP of 0.116 psid (shown in Figure 4.6) during the CWF indicates a lack of fouling on the filter (due to residual solids in the system). As such, these results indicate an overall clean system at the start of testing.

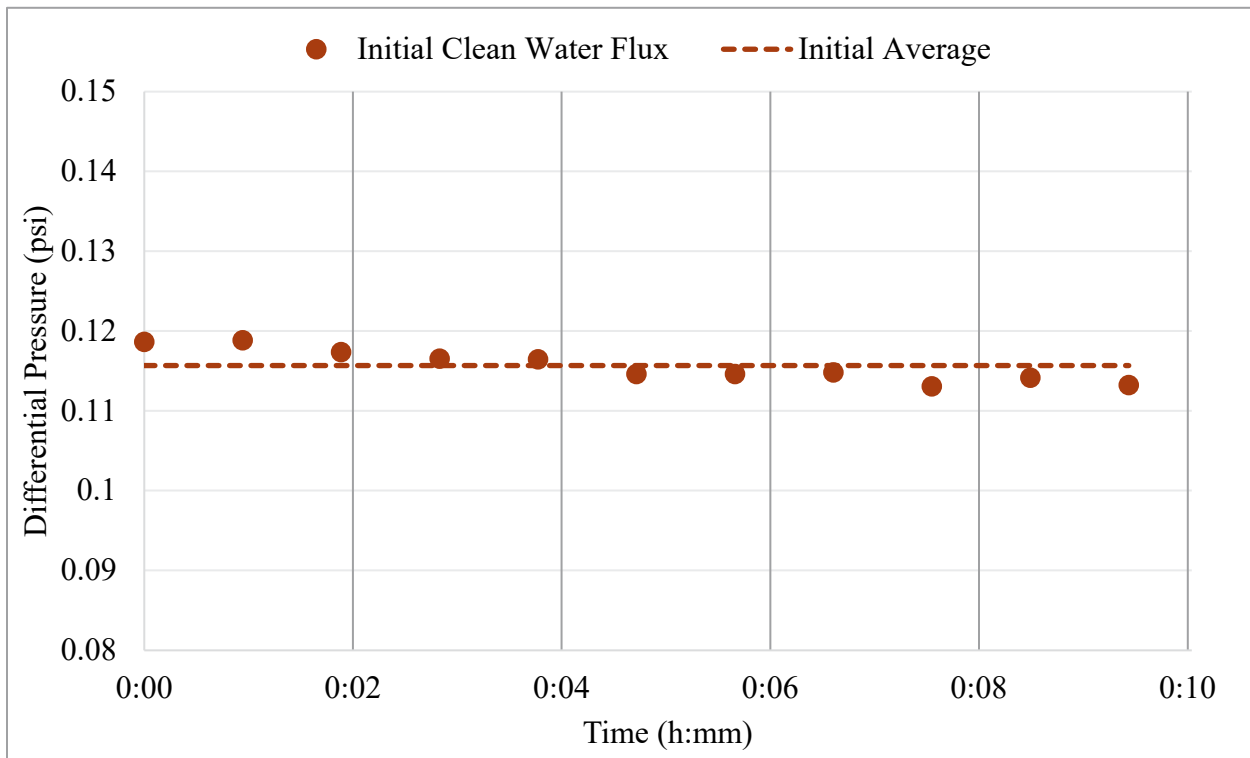


Figure 4.6. CWF measurements for Media Grade 5 BDEF at 2.57 mL/min (0.065 gpm/ft²) permeate rate (nominal) before testing. (Dashed line is average pressure over the 10-minute period.)

4.4 Waste Filtering

Each BDEF feed bottle was positioned in the trough heat exchanger to maintain feed temperature control ($16 \pm 1 \text{ }^\circ\text{C}$). Feed was then transferred into the BDEF reservoir via metering pump until approximately 2 in. of SY-101 solution remained in the feed bottle. The remaining “bottoms” from each feed bottle were consolidated and fed into the system toward the end of the filtration process. The filtration rate was

controlled via an MFC set at 2.57 mL/min (0.065 gpm/ft²). The actual flow rate averaged 2.54 mL/min. Slurry recirculation line pressure was kept between 20 and 25 psi, with adjustments made for any deviations. One backpulse was performed after the feed was exhausted. The 2-psi TMP limit (the threshold to indicate that a backpulse was needed) was not reached with the volume of feed tested.

Table 4.1 provides a timeline for the filtration testing, indicating feed bottle change, permeate bottle change and process liquid flow. Note that the filtration of feed bottle “bottoms” began after 5.00 m³/m² of feed had been filtered.

Table 4.1. System timeline.

Date	Time	Volume Filtered (m ³ /m ²)	Event
19-Mar	13:26	0.00	Filtration started with BDEF-SY1-1, dewatering into IX-SY1-1
	17:27	0.63	Filtering from feed bottle BDEF-SY1-2
	21:10	1.21	IX-SY1-1 full, dewatering into IX-SY1-2
	23:53	1.64	Filtering from feed bottle BDEF-SY1-3
20-Mar	3:31	2.20	Filtering from BDEF-SY1-4
	4:41	2.39	IX-SY1-2 full, dewatering into IX-SY1-3
	10:47	3.34	Filtering from BDEF-SY1-5
	11:57	3.53	IX-SY1-3 full, dewatering into IX-SY1-4
	15:27	4.07	Trough thermocouple (TE-104) pulled from BDEF-SY1-6 to BDEF-SY1-9
	15:47	4.13	Filtering from feed bottle BDEF-SY1-6
	18:50	4.61	Filtering from feed bottle BDEF-SY1-7
	19:40	4.74	IX-SY1-4 full, dewatering into IX-SY1-5
	21:03	4.95	Filtering from feed bottle BDEF-SY1-8
	21:22	5.00	Trough thermocouple (TE-104) pulled from BDEF-SY1-9 to BDEF-SY1-2 (consolidated bottoms bottle)
	22:22	5.16	Filtering from feed bottle BDEF-SY1-9
	22:38	5.20	Filtering from feed bottle BDEF-SY1-3 (consolidated bottoms from SY1-6, -7, -8)
21-Mar	3:02	5.89	IX-SY1-5 full, dewatering into IX-SY1-6
	4:07	6.06	Bubbles observed in feed bottle to reservoir transfer. Spacing clip removed from stinger so stinger could be lowered further into BDEF-SY1-3
	6:40	6.46	Trough thermocouple (TE-104) removed from BDEF-SY1-2 and transferred to BDEF-SY1-3 (consolidated bottoms bottle)
	7:36	6.61	Filtering from feed bottle BDEF-SY1-2 (consolidated bottoms from SY1-1, -2, -3, -4, -5)
	7:46	6.64	Noticed white solid particle floating in BDEF slurry reservoir
	10:36	7.08	IX-SY1-6 full, dewatering into IX-SY1-7
	16:27	8.00	Backpulse chamber filled from slurry reservoir
	16:34	8.00	Remainder of BDEF-SY1-3 (consolidated bottoms bottle) added to slurry reservoir
	16:39	8.01	TE-104 removed from BDEF-SY1-2 (consolidated bottoms bottle) and remainder added to slurry reservoir
	17:32	8.14	Pump speed reduced to 1250 rpm
	17:47	8.18	Pump speed reduced to 1000 rpm
	18:05	8.23	Pump speed reduced to 800 rpm. Filter differential pressure and flux unstable
	18:12	8.25	Chiller #2 setpoint increased from 5.5 C to 6.5 C
	19:05	8.39	Pump speed reduced to 600 rpm
19:12	8.40	IX-SY1-7 full, dewatering into IX-SY1-8	
19:50	8.50	V1 closed. End filtration	

Testing was started on the afternoon of March 19. During the initial filtration, TMP rapidly dropped from 0.5 to 0.127 psid at 0.12 m³/m² then recovered to 0.187 psid at 0.30 m³/m². Another TMP decay was observed from 0.187 psid at 0.30 m³/m² to 0.036 psid at 2.21 m³/m² and the TMP recovering to 0.124 psid at 2.22 m³/m². After this, TMP steadily increased to 0.158 psid at 8.0 m³/m² filtered as seen in Figure 4.7. At 8.0 m³/m², the backpulse chamber was filled in preparation for the final backpulse as the feed in the system was being exhausted. After this, a more rapid TMP increase was observed from 0.143 psid at 8.0 m³/m² to 0.242 psid at 8.47 m³/m². During this time, the recirculating pump speed was gradually decreased as feed levels in the slurry reservoir reached minimum operational volume. After this, the feed was exhausted at 8.50 m³/m², the test was ended, and the final backpulse was performed. See Table 4.2 for the system parameters prior to backpulse.

Table 4.2. Test parameters prior to backpulsing.

Test Event	Volume Filtered since Last		Transmembrane Pressure (psid)
	Filtration Resistance (1/m)	Backpulse (m ³ /m ²)	
Backpulse 1 ^(a)	9.48×10 ⁹	8.50	0.20

(a) Feed exhausted, TMP target not reached.

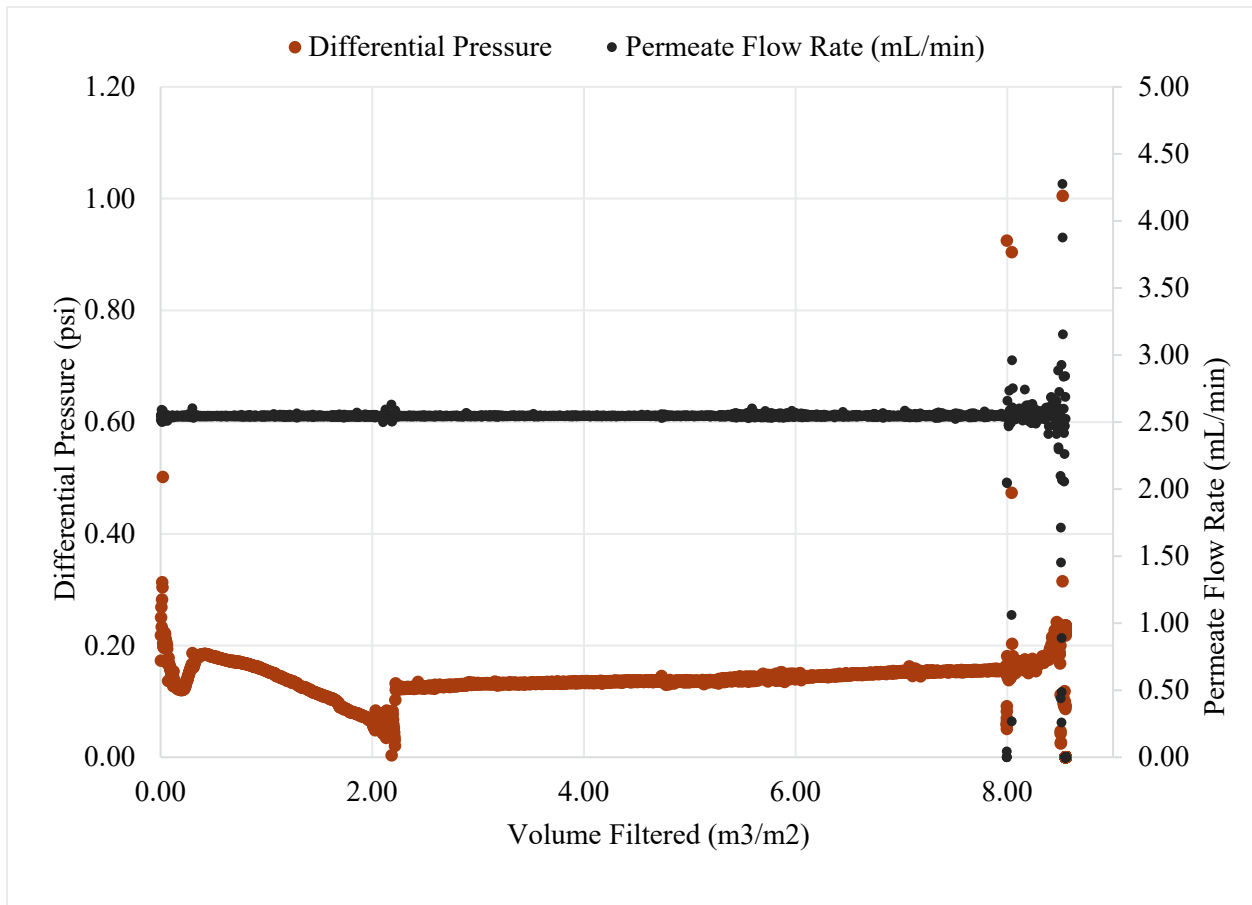


Figure 4.7. Filter differential pressure and MFC flow rate during filtering operations.

As stated before, Darcy’s law relates the flow rate through a porous media to the pressure drop causing that flow:

$$Q(t) = \frac{\Delta P}{(\mu * R(t))} \tag{4.3}$$

where Q is the filter volumetric flow rate, ΔP is the TMP, μ is the fluid viscosity, and R_{tot} is the total filtration resistance.

Rearranging produces:

$$R(t) = \frac{\Delta P}{(\mu * Q(t))} \tag{4.4}$$

Figure 4.8 shows this total filter resistance as a function of volume filtered over the 3 days of testing.

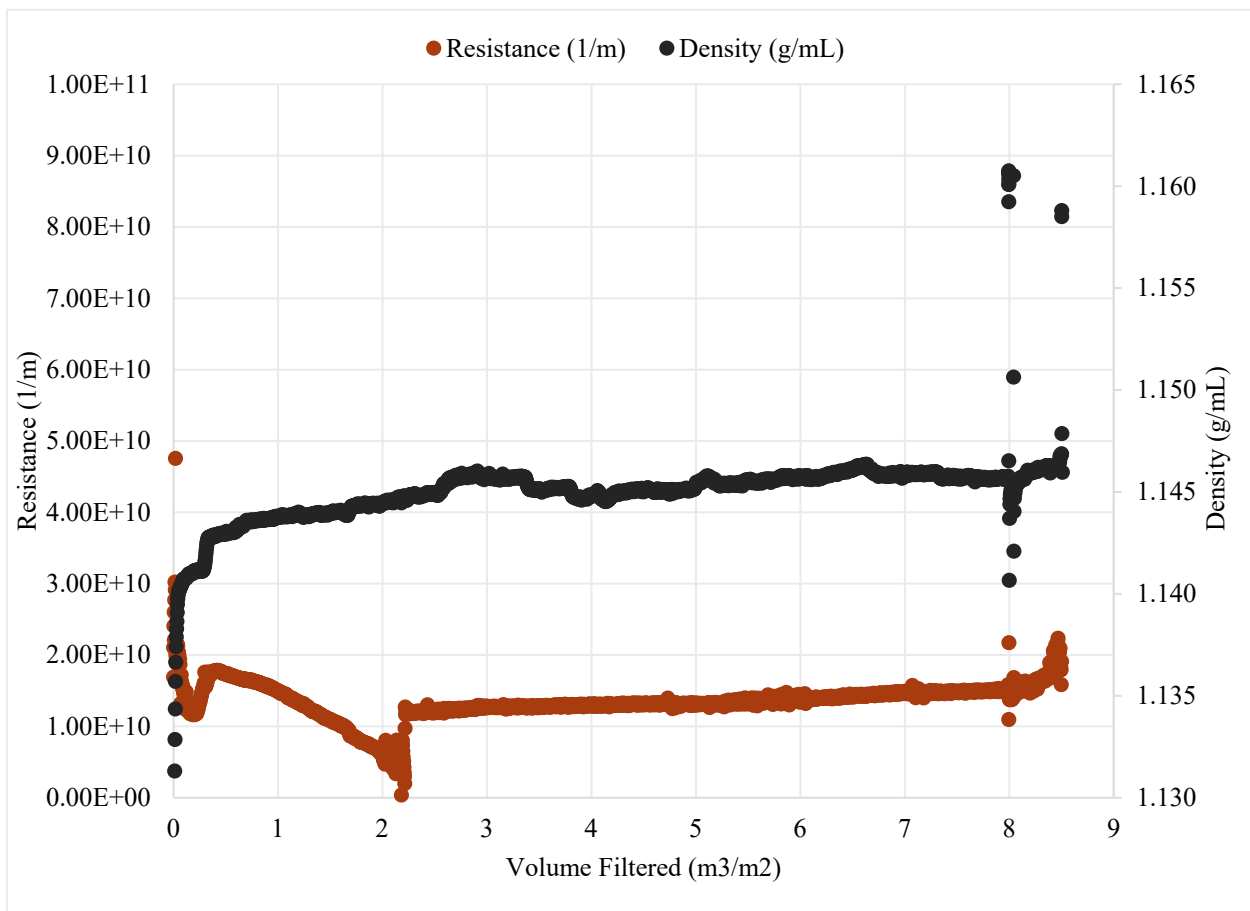


Figure 4.8. SY-101 filter resistance and permeate density during filtration process.

To assess the nature of the fouling occurring, multiple fouling mechanism functions were fit to the data using curve fit methodology developed in Hermia (1982) and applied in the FY20 AP-105 filtration testing detailed in RPT-DFTP-021 (Allred et al. 2020). The filtration laws developed by Hermia (1982) are for constant pressure DEF but can be readily recast into constant flux formulas as documented by Hlavacek and Bouchet (1993). For the present analysis, Hermia’s laws are recast into scaled resistance form, such that:

$$R^n = R_o^n (1 + \text{sign}(n) \sigma v) \quad (4.5)$$

Here, the exponent n defines the blocking regime, R scaled resistance, $v = V/A$ is the specific volume filtered, and σ is the regime dependent blocking parameter. In the present analysis, R_o is a reference resistance corresponding to the start of a given filtration period (either after startup or backflushing), and v is the specific volume filtered relative to that same reference point. The fouling mechanism is characterized by the value of n . Hermia (1982) defined four blocking regimes:

- Cake filtration blocking ($n = 1$)
- Intermediate blocking ($n = 0$)
- Standard blocking ($n = -0.5$)
- Pore / complete blocking ($n = -1$)

For the current data, a best-fit value of n is assessed for specific filtration periods using Microsoft Excel's built-in solver to minimize the root mean square error (RMSE) defined by:

$$\text{RMSE} = \sqrt{\sum_i (R_i^{(p)} - R_i^{(m)})^2} \quad (4.6)$$

where $R_i^{(p)}$ and $R_i^{(m)}$ are the predicted and measured resistances for an individual measurement i in the filtration period. To avoid the need to regress a best fit value of σ , it is estimated as:

$$\sigma = \frac{\text{sign}(n)}{v_f} \left[\left(\frac{R_f}{R_o} \right)^n - 1 \right] \quad (4.7)$$

where R_f and v_f are the final resistance and specific volume filtered of the period. Table 4.3 details the blocking parameters and regime exponent n determined by this analysis. The Table 4.3 results show evaluation of two filtration periods: the initial period of filtration and the period leading up to the first and only backflush.

Table 4.3. Filtration regime exponent n and blocking parameter σ .

Period	Regime Exponent n	Blocking Parameter σ , 1/m
Initial Fouling	1	0.0462
Backflush 1	-1	0.5590

The Table 4.3 results also indicate that the fouling behavior in the initial period exhibits filter resistance increases best characterized by cake fouling ($n = 1$) (see Figure 4.9 for this fit), suggesting solids are sufficiently large (from a hydrodynamic or chemical interaction basis) not to permeate into the depths of the filter. There is a transition in resistance increase that occurs at $8.0 \text{ m}^3/\text{m}^2$ right after the backpulse chamber was filled in preparation for the final backpulse. After that point, the fouling indicates a pore blocking behavior ($n = -1$), see Figure 4.10 for this fit. During the filling of the backpulse chamber, some solids on the surface could have started to make their way into the porous structure of the filter.

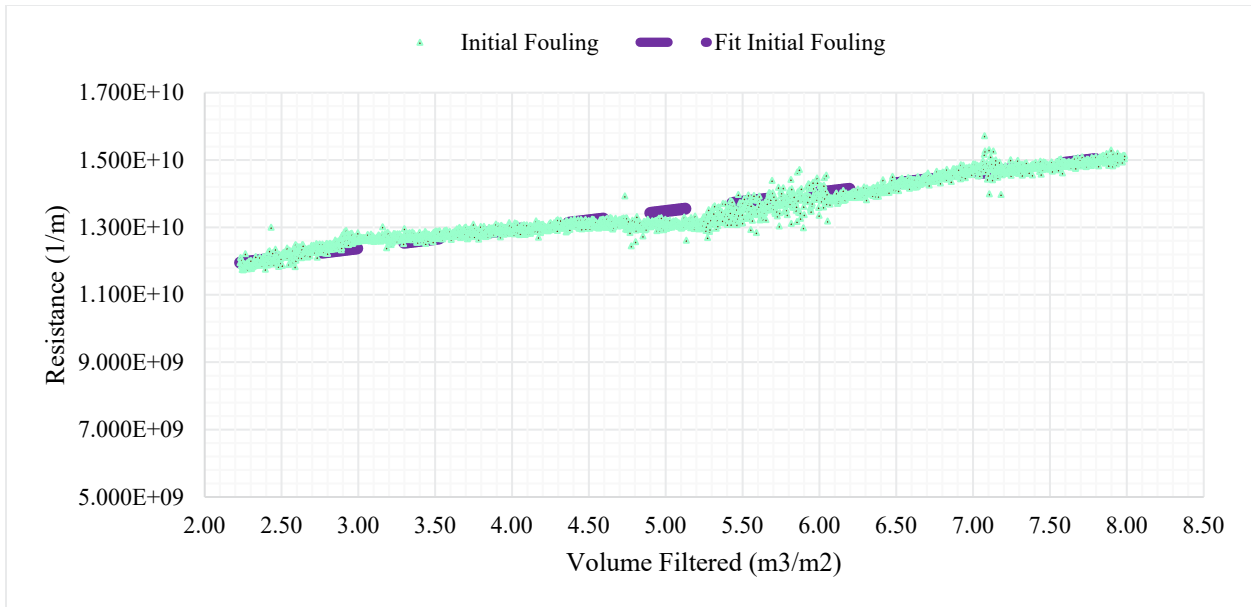


Figure 4.9. Fit to initial fouling experimental data using classical fouling mechanisms.

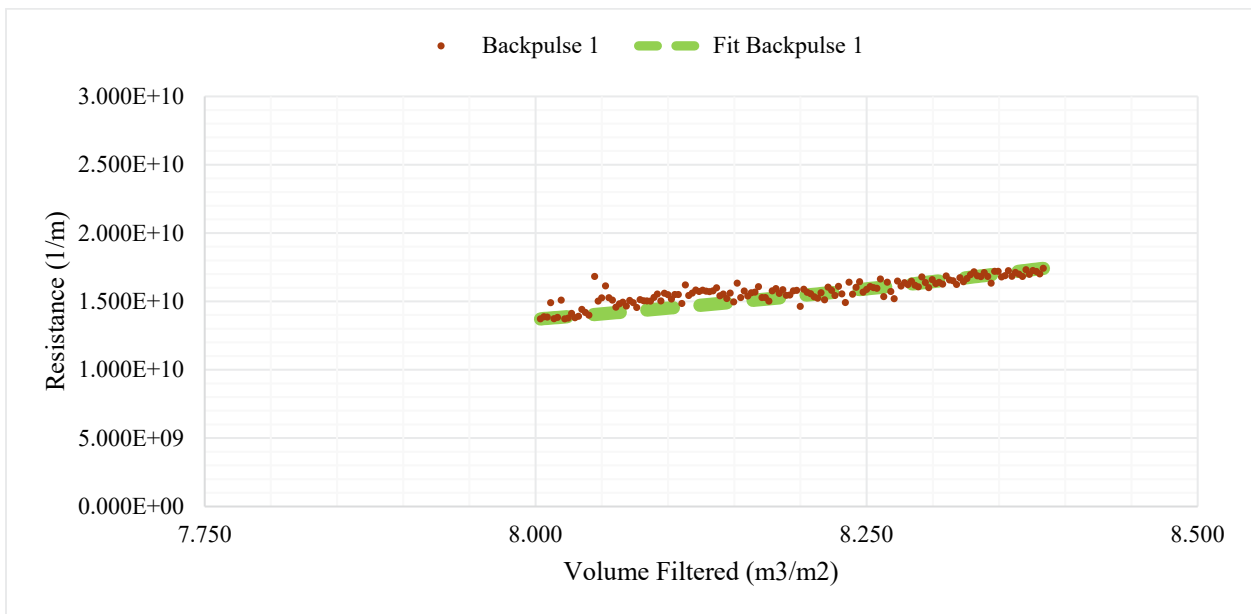


Figure 4.10. Fit to fouling prior to backpulse 1 experimental data using classical fouling mechanisms.

The density of the composited SY-101 solution ranged between approximately 1.140 and 1.147 g/mL per the MFC as shown in Figure 4.10 and averaged 1.145 g/mL through testing. No appreciable increase in density occurred upon the addition of the consolidated bottle “bottoms” to the slurry reservoir at 5.00 to 8.50 m³/m².

Post filtration analysis of the product bottles prior to IX included the measurement of product density. Density measurement was performed in a 10-mL volumetric flask at 25.4 °C. These values are reported in Table 4.4 and show little variation in density between bottles. Average bottle density was found to be 1.1320 g/mL with a standard deviation of 0.0048 g/mL and percent relative standard deviation of 0.42%.

Table 4.4. Post filtration density measurements of product bottles.

Bottle ID	Density (g/mL)
IX-SY1-1	1.1284
IX-SY1-2	1.1316
IX-SY1-3	1.1319
IX-SY1-4	1.1339
IX-SY1-5	1.1330
IX-SY1-6	1.1402
IX-SY1-7	1.1248

4.5 Final CWF

At the conclusion of SY-101 filtration, a filter cleaning was performed, and the CWF was measured again. Figure 4.11 compares this final CWF with the initial CWFs. The filter differential pressure of the final CWF at 15.6 °C was averaged to be 0.110 psid. This sits just below the initial CWF average TMP, which was 0.116 psid. This indicates filter cleaning dissolved all of the solids that were deposited on the filter during testing.

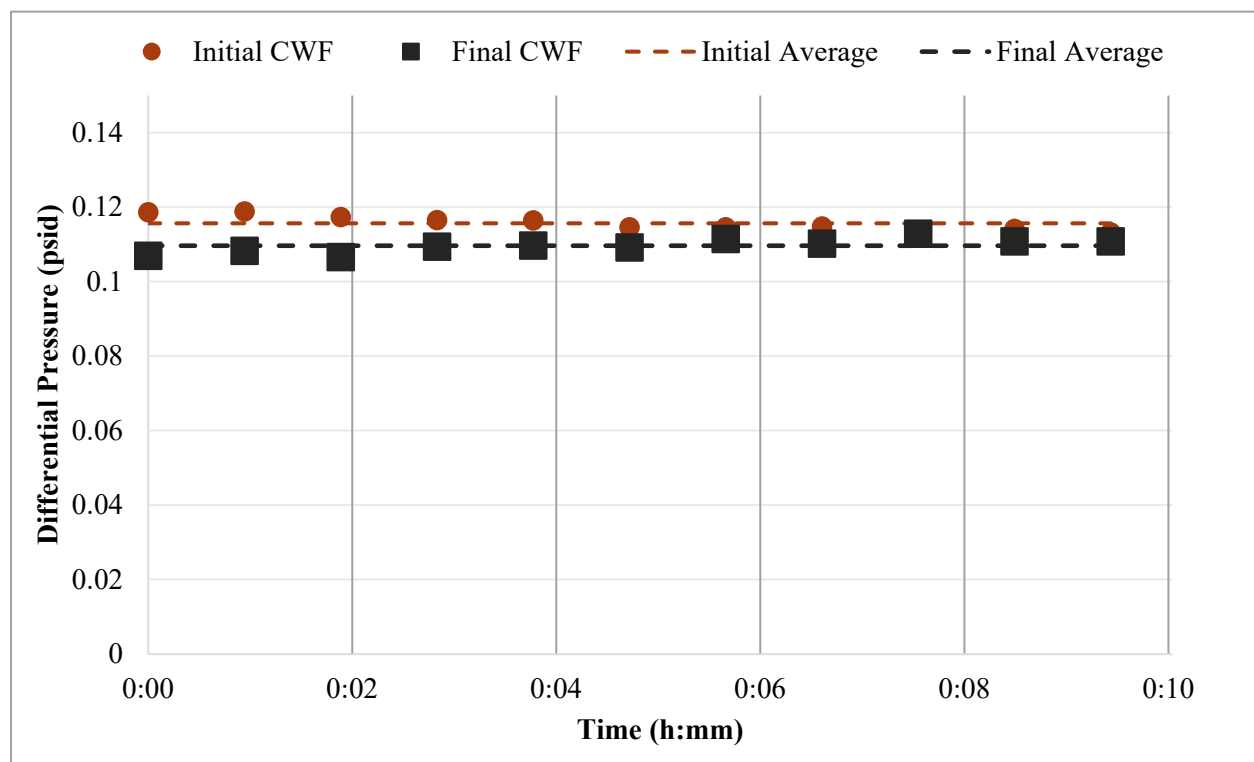


Figure 4.11. Initial and final clean water flux.

4.6 Analytical Results

4.6.1 Compositing SY-101 Supernate Tank Waste Analysis

Inductively coupled plasma-optical emission spectroscopy (ICP-OES) analysis was conducted on the composited SY-101 supernate tank waste on a mass-per-unit-mass basis ($\mu\text{g/g}$) as presented in Table 4.5. Subsequently, the molarity of the composited waste was calculated using a density of 1.126 g/mL, which was determined after sample composite completion of the SY-101 tank waste. The detailed ICP-OES report is found in Appendix D.

The molarity was calculated using the following equation:

$$M = \frac{(m * \rho)}{MW} \quad (4.8)$$

where M is the molarity, m is the mass, ρ is the density, and MW is the molecular weight of the component.

Table 4.5. ICP-OES results of composited SY-101 supernate tank waste.

Analysis Method	Analyte	Composited SY-101 ($\mu\text{g/g}$)	Composited SY-101 Molarity (mol/L)
ICP-OES	Na	57,850	2.83E+00
	Al	3,315	1.38E-01
	P	2,305	8.38E-02
	S	610	2.14E-02
	K	348	1.00E-02
	Cr	98	2.12E-03

4.6.2 Total Alpha Energy Analysis

Total alpha analysis (alpha energy analysis, AEA) was conducted to determine the TRU content of the filtered permeate. The analysis results are given in Table 4.6 and show no gross breakthrough of TRU components that aren't already soluble. Additional detail is provided in Appendix C. All samples remained below the 0.1 $\mu\text{Ci/g}$ threshold defining TRU waste per DOE M 435.1-1, *Radioactive Waste Management Manual*. The third permeate sample did show a higher alpha concentration, likely due to the consolidation of the product feed bottoms throughout filtration, as discussed in Section 4.4.

Table 4.6. AEA for permeate samples.

Analysis Method	Sample ID	IX Product Bottle Sampled From	($\mu\text{Ci/mL}$)	($\mu\text{Ci/g}$)
Total alpha analysis	TI-145-P1	IX-SY1-1	3.65E-5	3.24E-5
	TI-145-P2	IX-SY1-3	2.59E-5	2.30E-5
	TI-145-P3	IX-SY1-8	4.52E-5	4.01E-5

4.6.3 Rheology Analysis of Filtered and Cesium Decontaminated SY-101 Supernate Tank Waste

The viscosity of the filtered and cesium exchanged SY-101 supernatant was measured with a Haake M5-RV20 (equipped with an M5 measuring head and RC20 controller) and an MV1 rotor and cup measuring system. Temperature was controlled using a combination of the standard measuring system temperature jacket and a NESLAB temperature-controlled circulator, Model Number RTE 111. This circulator allows heating and cooling of recirculation fluid to the rheometer over a range of -25 to 150 °C with a stability of $\pm 0.01^\circ \text{C}$. Performance checks using a Cannon-certified viscosity reference standard (Cannon Instrument Company) were carried out prior to and after measurements to verify that the system was functioning as expected. Viscosity was measured using a standard flow curve protocol comprising an up-ramp from 0 to 1000 s^{-1} for 5 minutes, a hold of 60 seconds at 1000 s^{-1} , and a finally down-ramp from 1000 to 0 s^{-1} over 5 minutes. Flow curves were measured at four temperatures: 10, 16, 25, and 35 °C. For each temperature, the Newtonian viscosity¹ of the liquid was determined by linear regression of the down-ramp data. The range of fit shear rates was generally limited to shear rates greater than 50 s^{-1} and below 600 s^{-1} to exclude data impacted by onset of secondary flows (i.e., Taylor vortices). The results of linear regression analysis and the resulting best fit Newtonian viscosities are reported in Table 4.7. In all cases, the measured viscosity of the SY-101 supernatant is below the recommended range of the measuring system (nominally 5.5 to 650 mPa s).

Table 4.7. Viscosity results of filtered and Cs decontaminated sample.

Temperature (°C)	Fit Range	Viscosity	Viscosity
	Down-Ramp, s^{-1}	mPa s	Uncertainty ^(a) 3-Sigma Relative % Standard Error
10	50-400	2.90	0.09
16	50-450	1.6	0.2
25	N/A	N/A	N/A
35	N/A	N/A	N/A

(a) The uncertainty reported by the Haake software for the curve fit is the 3-sigma relative percent standard error.

4.7 Microscopy Solids Analysis

Material collected from the concentrated backpulse solution was submitted for examination by scanning transmission electron microscopy (STEM) imaging, X-ray energy dispersive spectroscopy (EDS), transmission electron microscopy (TEM), and selected area electron diffraction (SAED). A full report of the particle imaging and analysis can be found in Appendix E. The samples analyzed were received as a liquid with suspended solids that had been centrifuged to concentrate the solids. Samples for microscopy analyses were prepared using a filtering method to avoid as much as possible the formation of evaporative salts. The solutions were wicked through a lacey carbon with a support TEM grid made of copper. Some prepared TEM grids were also examined with scanning electron microscopy (SEM) for morphology and particle size analysis and with STEM. SY-101 was previously analyzed by Liu et al. (1995) at PNNL, where they concentrated on examining the Al phases. Compositional analysis from the sample used in

¹ While the SY-101 supernatant is expected to be Newtonian, linear regression analysis allowed for non-zero intercept to accommodate a non-zero torque offset introduced by the operator to accommodate negative torques resulting from operating the M5 viscometer outside its standard operating range (in this case, for viscosities below 5.5 mPa s).

this study indicated that as well as Na and Al, P and Cr would potentially be major components in the any solids present.

Large particles, more than 200 μm across, were observed occasionally; however, it was not possible to analyze these with STEM analysis. With SEM, the very large particles could be easily accommodated but the STEM/TEM analysis was limited to particles <20-50 μm in diameter. Indeed, some of the large particles had to be physically removed from the TEM grid prior to introduction in the STEM chamber.

The large, agglomerated particles shown in Figure 4.12 were commonly found throughout the SY-101 samples prepared by the filtering method. Some of the smaller agglomerates were examined by STEM.

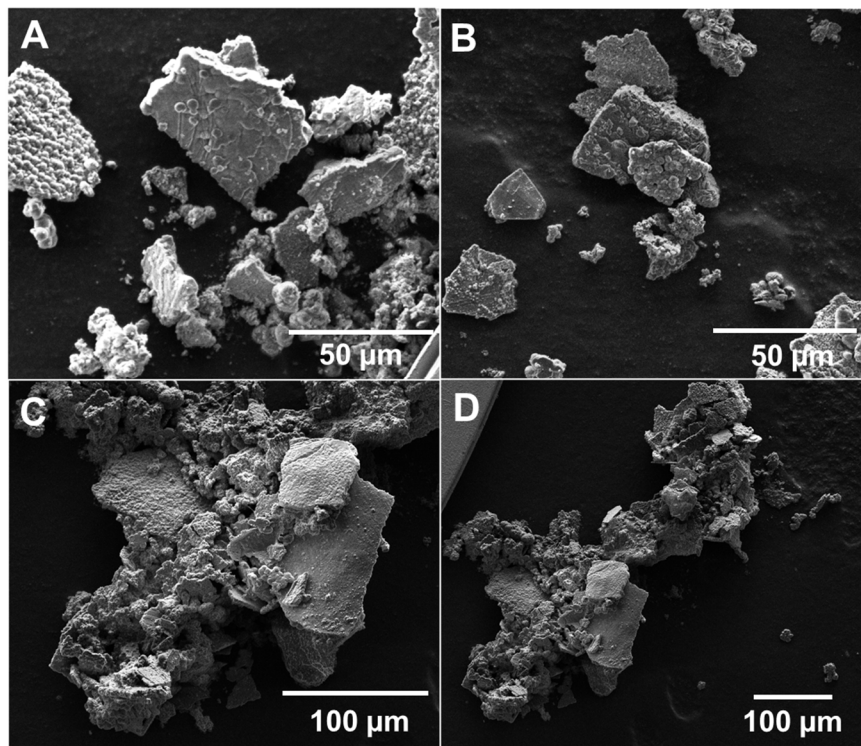


Figure 4.12. (A-D) SEM images of SY-101 solids showing a variety of morphologies and agglomerates, in some instances, >200 μm in diameter.

Figure 4.13 shows STEM-HAADF (high-angle annular dark-field), and the TEM image from the same region. The red arrows indicate the rotation in the image between the STEM and TEM images. The orange circles represent where SAED patterns were obtained (see Appendix E, Figure E.1 for further information). Most of the agglomerate was found to be electron beam amorphous. The STEM EDS elemental maps of the agglomerated particle showed the occurrence of aluminum oxide, chromium-bearing, iron, and calcium phosphate particles. In most instances, the collected electron diffraction patterns could not be indexed as they either did not show enough reflections or appeared to be amorphous.

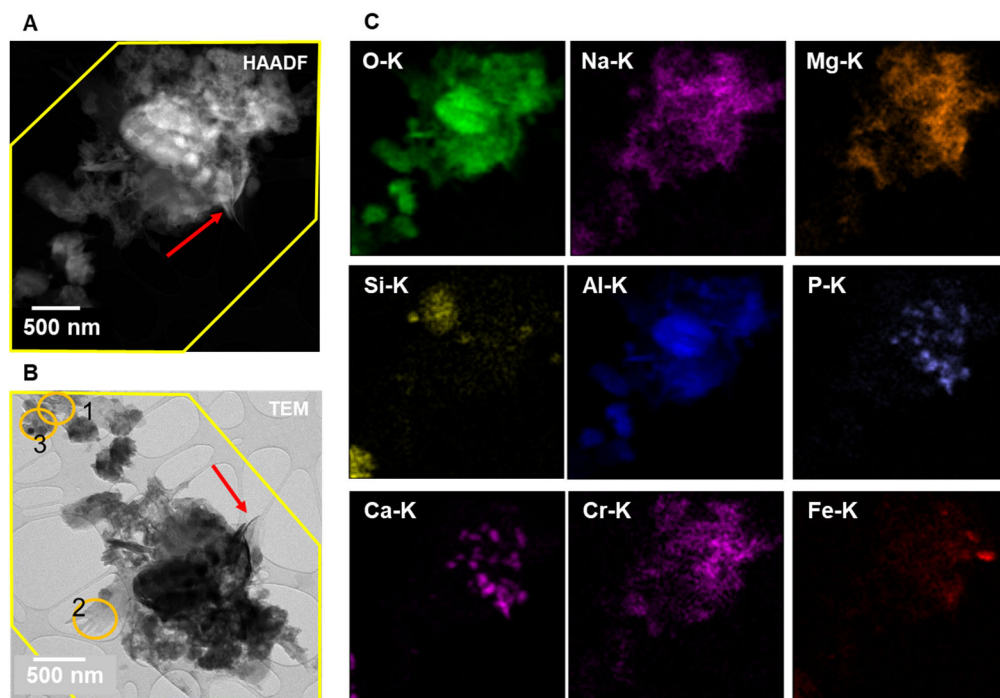


Figure 4.13. (A) Medium magnification STEM image and (B) TEM image of the same region (indicated by the red arrow) showing regions where SAED were collected (orange circles and shown in Figure D.2), and (C) STEM-EDS maps showing the occurrence of aluminum oxide, chromium-bearing phase, iron particle, and calcium phosphate phase.

Figure 4.14 shows TEM SAED and STEM-EDS elemental maps of another particle agglomerate. In this case, the diffraction patterns shown in Figure 4.14A and B were analyzed with CrysTBox software (Klinger 2017) using potential matches from the American Mineralogist Crystallographic Database (<http://rruff.geo.arizona.edu/AMS/amcsd.php>) for apatite for the calcium phosphate phase and boehmite for the nanocrystalline Al-rich phase. The STEM-EDS elemental maps are slightly misaligned relative to the TEM image. The dark particle (indicating that it is close to a major zone axis) was the apatite particle (Ca-phosphate). Calcium phosphate particles were also observed throughout the sample (see Figure 4.13 and Appendix E, Section E.1). The Al-phase was barely crystalline but was observed frequently in the sample. Further analysis of this phase is described in Section E.1. The phase did appear to contain Cr (see Table 4.8). The match to apatite was good but the match to the selected aluminum oxide phase, boehmite, was questionable (see Table 4.9). Both the SAED pattern and the fast Fourier transform (FFT) from the high-resolution TEM image were used to describe the structure of the phase.

The SY-101 grids were examined in the SEM for particle analysis sizing. The results of this analysis are described in Section E.2.

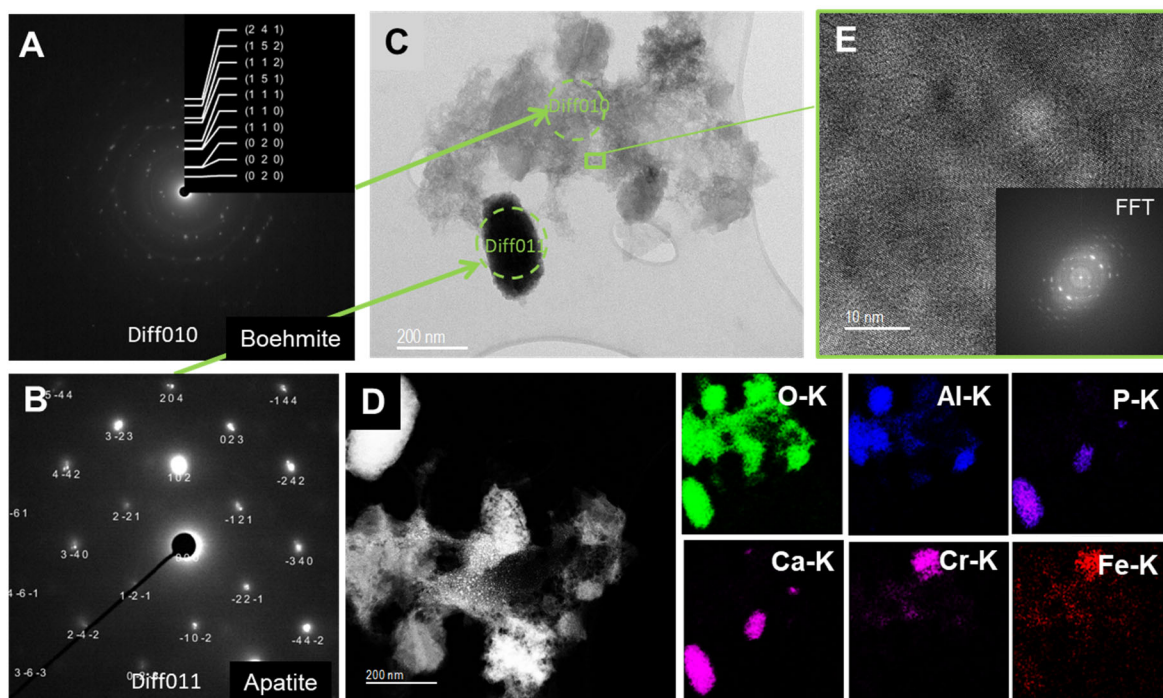


Figure 4.14. (A) Electron diffraction of Al-phase matched to boehmite, (B) electron diffraction pattern of apatite, (C) TEM image of a nano-structured material revealed with indicated regions where SAED were obtained, (D) STEM-HAADF of the same region, (E) high-resolution TEM of Al-phase indicating crystallinity (see insert FFT), and STEM-EDS maps of O, Al, P, Ca, Cr, and Fe.

Figure 4.15 shows the varied types of particles imaged with SEM that were found in the SY-101 solids sample. Many of the particles were irregularly shaped. Their ability to be trapped by the holey carbon film used in the analysis might be similar to their ability to be trapped on the dead-end filter.

Table 4.8. Compositional analysis of Cr-bearing Al-phase.

Element	Counts	Atomic%
Na K	1471	3.25
Mg K	11484	16.76
Al K	42883	69.14
Si K	969	3.61
P K	1683	4.03
Ca K	1450	0.77
Ti K	750	0.24
Cr K	6677	1.23
Mn K	402	0.06
Fe K	2765	0.32
Co K	1730	0.16
Ni K	5490	0.40
		100.00

Table 4.9. Electron diffraction from Cr-bearing Al-phase.

Plane	d-spacing (nm) (theor)	d-spacing (nm) (measured)	d-spacing (nm) (FFT)
(0 2 0)	0.612	0.756	0.8379
(0 2 0)	0.612	0.472	0.4190
(0 2 0)	0.612	0.460	--
(1 1 0)	0.280	0.270	0.2791
(1 1 0)	0.280	0.264	--
(1 1 1)	0.223	0.225	0.2331
(1 5 1)	0.167	0.166	0.1851
(1 1 2)	0.155	0.156	0.1537
(1 5 2)	0.131	0.133	--
(2 4 1)	0.123	0.124	--

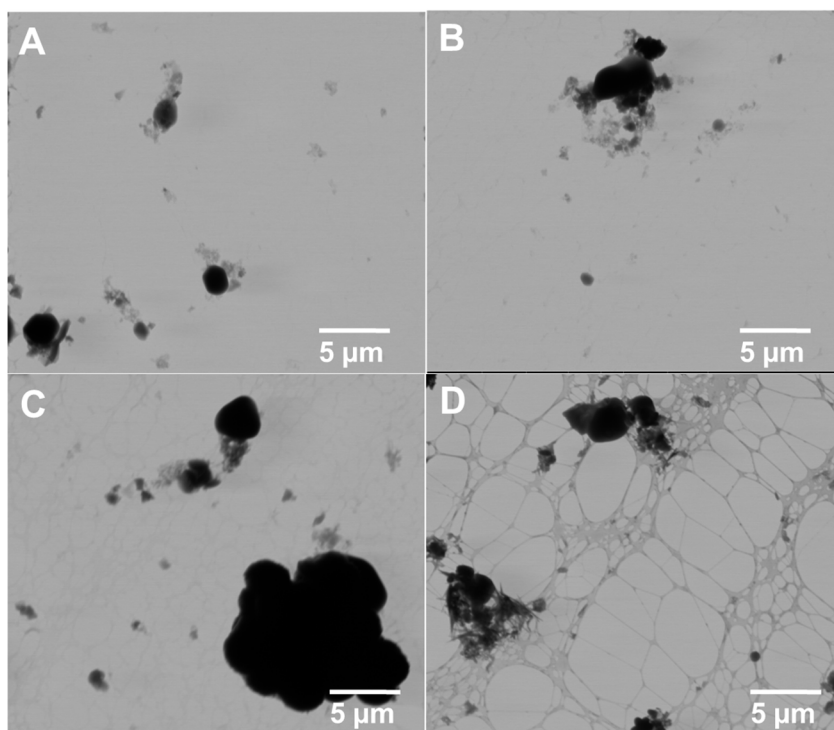


Figure 4.15. SEM image using a STEM detector showing different morphologies of particles from the SY-101 sample. Analysis excluded the very large particles shown in Figure 4.9.

5.0 Conclusions

Based on the results of the filtration experiments on supernatant waste from tank 241-SY-101 at 16 °C, the following observations and conclusions were made:

- During filtration, the differential pressure required to effect filtration at 0.065 gpm/ft² increased little over the filtration campaign and never reached 2 psid (the TSCR action limit). This indicates that the Media Grade 5 filter should perform well when processing SY-101 supernatant.
- The prototypic filter cleaning process effectively restored filter performance.
- Solids concentrated from the backpulse solutions were composed of aluminum oxide, chromium, and calcium phosphate that occurred as particle agglomerates. There was less evidence of fine salt-like particles in this sample than seen in prior tests (Allred et al. 2020).

6.0 References

- Allred JR, EC Buck, CC Burns, RC Daniel, JGH Geeting, ZB Webb, AM Westesen, and RA Peterson. 2022. *Fiscal Year 2022 Filtration of Hanford Tank 241-AP-101 Supernatant at 16 °C*. PNNL-32851, Rev. 0 (RPT-DFTP-032, Rev. 0). Pacific Northwest National Laboratory, Richland, Washington.
- Allred JR, JGH Geeting, AM Westesen, EC Buck, and RA Peterson. 2020. *Fiscal Year 2020 Filtration of Hanford Tank Waste 241-AP-105*. PNNL-30485, Rev. 0 (RPT-DFTP-021, Rev. 0). Pacific Northwest National Laboratory, Richland, Washington.
- ASME. 2000. *Quality Assurance Requirements for Nuclear Facility Applications*. NQA-1-2000. The American Society of Mechanical Engineers, New York, New York.
- ASME. 2008. *Quality Assurance Requirements for Nuclear Facility Applications*. NQA-1-2008. The American Society of Mechanical Engineers, New York, New York.
- ASME. 2009. *Addenda to ASME NQA-1-2008*. NQA-1a-2009. The American Society of Mechanical Engineers, New York, New York.
- Detrich, EJ. 2019. *Derivation of Best-Basis Inventory for Tank 241-SY-101 as of October 1, 2020*. RPP-RPT-48774, Rev. 4. Washington River Protection Solutions, Richland, WA.
- Gerber MS. 1992. *Legend and Legacy: Fifty Years of Defense Production at the Hanford Site*. WHC-MR-0293, Rev. 2. Westinghouse Hanford Company, Richland, Washington. doi:10.2172/10144167
- Hlavacek, M., Bouchet, F. (1993) Constant flux rate blocking laws and an example of thief application to dead-end microfiltration of protein solutions. *J. Membr. Sci.*, 82: 285-295.
- Hermia J. 1982. "Constant Pressure Blocking Filtration Laws – Application to Power-Law Non-Newtonian Fluids." *Transactions of the Institution of Chemical Engineers* 60(3):183-187.
- Klinger M. 2017. "More features, more tools, more CrysTBox." *Journal of Applied Crystallography* 50(4):1226-1234. <https://doi.org/doi:10.1107/S1600576717006793>
- Liu, J., L. R. Pederson, and L. Q. Wang. 1995. *Solid-Phase Characterization in Flammable-Gas-Tank Sludges by Electron Microscopy*. PNL-10723, Pacific Northwest Laboratory, Richland, Washington.

Appendix A – BDEF Piping and Instrumentation Diagram

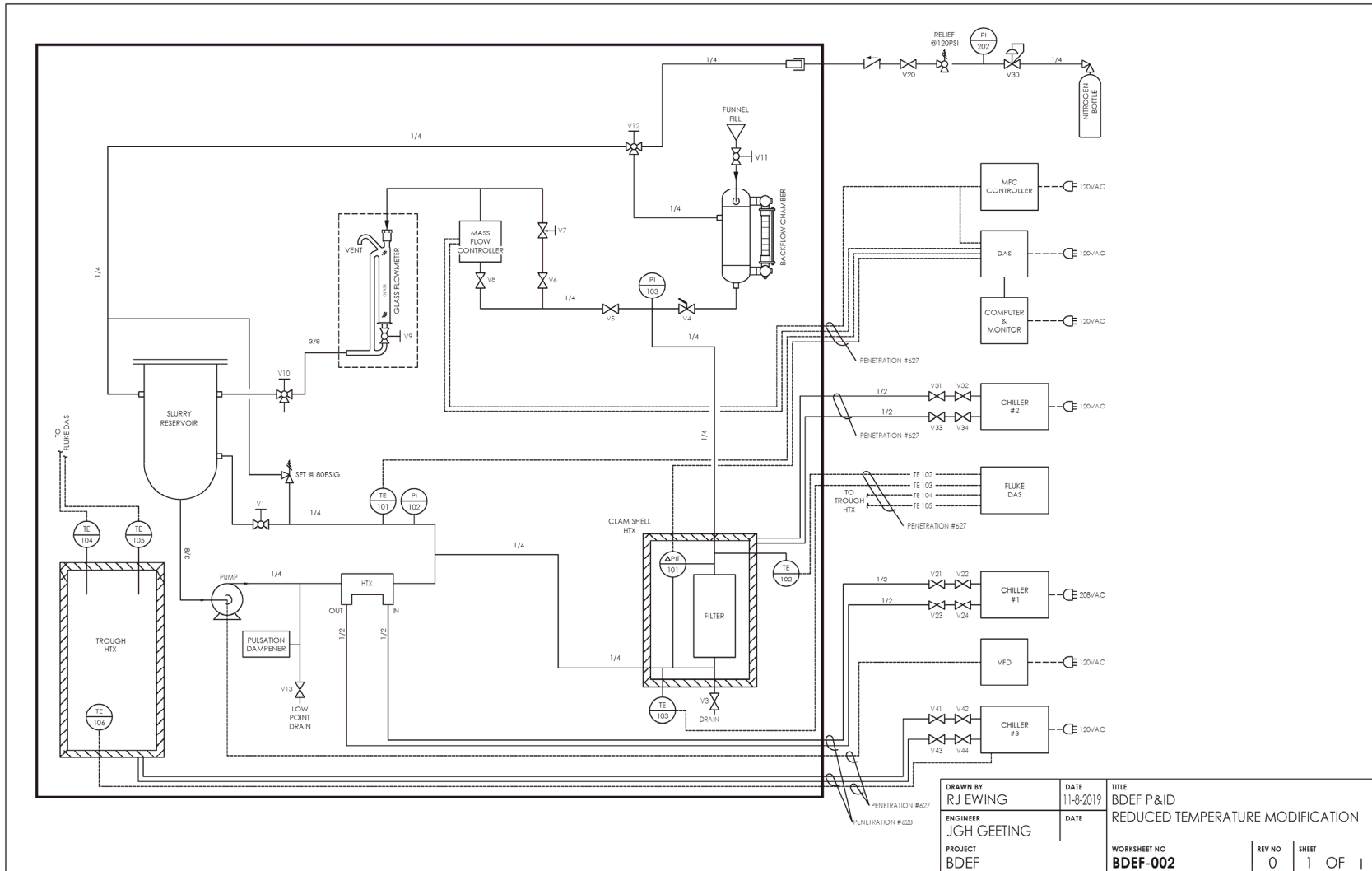


Figure A.1. BDEF piping and instrumentation diagram.

Appendix B – Feed Bottle Composite

Composite Bottle ID	Receipt Sample Bottle ID	Sample Location (depth below liquid surface, inches)	Mass Addition to Composite Bottle (g)
BDEF-SY1-1	1SY-23-01	26	207.64
	1SY-23-07	81	206.04
	1SY-23-13	135	206.8
	1SY-23-19	187	210.3
	1SY-23-25	240	211.81
	1SY-23-31	294	216.43
BDEF-SY1-2	1SY-23-02	26	214.86
	1SY-23-08	81	213.7
	1SY-23-14	135	217.86
	1SY-23-20	187	219.41
	1SY-23-26	240	213.32
	1SY-23-32	294	213.05
BDEF-SY1-3	1SY-23-03	26	214.13
	1SY-23-09	81	216.15
	1SY-23-15	135	214.78
	1SY-23-21	187	206.19
	1SY-23-27	240	209.72
	1SY-23-33	294	213.95
BDEF-SY1-4	1SY-23-04	26	211.05
	1SY-23-10	81	211.8
	1SY-23-16	135	209
	1SY-23-22	187	213.38
	1SY-23-28	240	220.19
	1SY-23-34	294	228.45
BDEF-SY1-5	1SY-23-05	26	214.31
	1SY-23-11	81	224.38
	1SY-23-17	135	211.89
	1SY-23-23	187	214.46
	1SY-23-29	240	211.98
	1SY-23-35	294	219.49
BDEF-SY1-6	1SY-23-06	26	217.34
	1SY-23-12	81	221.07
	1SY-23-18	135	208.18
	1SY-23-24	187	215.26
	1SY-23-30	240	217.79
	1SY-23-36	294	219.87
BDEF-SY-7	1SY-23-01	26	56.04
	1SY-23-07	81	56.32
	1SY-23-13	135	54.83
	1SY-23-19	187	59.63
	1SY-23-25	240	57.17
	1SY-23-31	294	54.86
	1SY-23-02	26	58.91
	1SY-23-08	81	55.32
	1SY-23-14	135	55.53
	1SY-23-20	187	43.47
	1SY-23-26	240	55.02
	1SY-23-32	294	62.05

Composite Bottle ID	Receipt Sample Bottle ID	Sample Location (depth below liquid surface, inches)	Mass Addition to Composite Bottle (g)	
BDEF-SY-8	1SY-23-03	26	57.86	
	1SY-23-09	81	54.38	
	1SY-23-15	135	57.24	
	1SY-23-21	187	68.3	
	1SY-23-27	240	53.85	
	1SY-23-33	294	67.21	
	1SY-23-04	26	56.33	
	1SY-23-10	81	63.82	
	1SY-23-16	135	57.13	
	1SY-23-22	187	37.51	
	1SY-23-28	240	42.22	
	1SY-23-34	294	46.88	
	BDEF-SY-9	1SY-23-05	26	58.07
		1SY-23-11	81	47.08
1SY-23-17		135	55.38	
1SY-23-23		187	53.98	
1SY-23-29		240	58.43	
1SY-23-45		294	55.06	
1SY-23-06		26	52.41	
1SY-23-12		81	48.99	
1SY-23-18		135	48.41	
1SY-23-24		187	51.6	
1SY-23-30		240	48.05	
1SY-23-36		294	42.23	

Appendix C – Total Alpha Analysis for Filtration Permeate Samples

Pacific Northwest National Laboratory
Richland, WA
Radiochemical Sciences and Engineering Group

filename ASR 1726 Allred report
6/2/2023

Client: Allred Project: 79156
ASR: 1726 WP: NN2047

Prepared by: Truc Trang-Le Digitally signed by Truc Trang-Le
Date: 2023.06.02 14:23:09 -0700'

Concur: Lawrence R Greenwood Digitally signed by Lawrence R
Greenwood
Date: 2023.06.02 14:20:30 -0700'

Procedures: Activity #4668 Source Preparation for Gross Alpha and Gross Beta Analysis
Activity #6343 Total Alpha and Total Beta Analysis
M&TE Ludlum
Count date: May 31 & June 1, 2023

Sample	Lab ID	Measured Activity, $\mu\text{Ci/g} \pm 1s$	
		Gross alpha	
TI-145-P1	23-0824	4.19E-05	± 23%
	23-0824 DUP	3.10E-05	± 30%
TI-145-P2	23-0825	2.59E-05	± 49%
TI-145-P3	23-0826	4.52E-05	± 23%
	Blank Spike	101%	
	Matrix spike	103%	

Appendix D – ICP-OES Analysis for As-Received 241-SY-101 Supernatant

Battelle PNNL/RPL/Inorganic Analysis ... ICP-OES Analysis Report

Project / WP#: 81126 / NP1205
 ASR#: 1673
 Client: A. Westesen
 Total Samples: 1 (liquid)

ASO Sample ID	Client Sample ID	Client Sample Description
23-0331	1SY-23-COMP	SY-101 Tank Waste Supernate
Sample Preparation: Simple dilution of "as received" samples in 5% v/v HNO ₃ performed by C. Perez.		

Procedure: <u>RPG-CMC-211_Rev_4</u> , "Determination of Elemental Composition by Inductively Coupled Argon Plasma Optical Emission Spectrometry (ICP-OES)."					
Analyst:	C. Perez	Analysis Date:	3/23/2023	ICP File:	C0901
See Chemical Measurement Center 98620 file: <u>ICP-325-405-3</u> (Calibration and Maintenance Records)					
M&TE:	<input checked="" type="checkbox"/>	PerkinElmer 5300DV ICP-OES	SN: 077N5122002		
	<input type="checkbox"/>	Sartorius ME414S Balance	SN: 21308482		
	<input type="checkbox"/>	Mettler AT400 Balance	SN: 1113162654		
	<input type="checkbox"/>	Sartorius R200D Balance	SN: 39080042		
	<input type="checkbox"/>	Mettler AT201 Balance	SN: 192720-92		
	<input checked="" type="checkbox"/>	Ohaus Pioneer PA224C	SN: B725287790		
	<input type="checkbox"/>	SAL Cell 2 Balance	SN: 8033311209		

Christian Perez

Digitally signed by Christian Perez
Date: 2023.06.23 14:27:04 -07'00'

Report Preparer

Steven Baum

Digitally signed by Steven Baum
Date: 2023.06.27 12:11:54 -07'00'

Review and Concurrence

Battelle PNNL/RPL/Inorganic Analysis ... ICP-OES Analysis Report

One aqueous sample was submitted under Analytical Service Request (ASR) 1673 was analyzed by ICP-OES. The sample had an acid digestion performed and was done in combination with samples from ASR 1672.

All sample results are reported on a mass per unit volume basis ($\mu\text{g/mL}$) for each detected analyte. The data have been adjusted for instrument dilutions.

Analytes of interest (AOI) were specified in the ASR and are listed in the highlighted section of the attached ICP-OES Data Report. The quality control (QC) results for the AOI have been evaluated and are presented below.

Calibration of the ICP-OES was done following the manufacturer's recommended calibration procedure using multi-analyte custom standard solutions traceable to the National Institute of Standards and Technology (NIST). Midrange calibration verification standards (MCVA and MCVB) were used to verify acceptance of the two-point calibration curves obtained for each analyte and for continuing calibration verification.

The controlling documents were procedures RPG-CMC-211, Rev 4, *Determination of Elemental Composition by Inductively Coupled Argon Plasma Optical Emission Spectrometry (ICP-OES)*, and ASO-QAP-001, Rev. 11, *Analytical Support Operations (ASO) Quality Assurance Plan*. Instrument calibrations, QC checks and blanks (e.g., ICV/ICB, CCV/CCB, LLS, ICS), post-digestion spikes, duplicate, blank spike, and serial dilution were conducted during the analysis run.

Preparation Blank (PB):

A preparation blank was supplied with the samples. All AOI were within the acceptance criteria of $< \text{EQL}$ (estimated quantitation level), $< 50\%$ regulatory decision level, or less than $\leq 10\%$ of the concentration in the sample.

Blank Spike (BS)/Laboratory Control Sample (LCS):

A 50:50 mixture of the MCVA and MCVB solutions was analyzed as the blank spike. Recovery values are listed for all analytes included in the BS that were measured at or above the EQL. All AOI meeting this requirement were within the acceptance criterion of 80% to 120%.

Duplicate/Replicate Relative Percent Difference (RPD):

A Replicate of each sample was prepared and analyzed. RPD are listed for all analytes that were measured at or above the EQL. All AOI were within the acceptance criterion of $\leq 20\%$ for liquid samples.

Triplicate Relative Standard Deviation (RSD):

No triplicate sample was analyzed.

Battelle PNNL/RPL/Inorganic Analysis ... ICP-OES Analysis Report

Matrix-Spike (MS) Sample:

The samples were analyzed "as received" and diluted as appropriate for analyses of the target analytes. A matrix spike sample was generated due to the sample preparation beforehand labeled as MS-23-0331. Potassium (K) and Aluminum (Al) passed on the recovery percentage. Sodium (Na) shows as "nr" on the percentage recovered. This concludes that the spike concentration is <25% of the sample concentration which gives inconclusive results for Sodium.

Initial/Continuing Calibration Verification (ICV/CCV):

MCVA and MCVB solutions were analyzed immediately after calibration, after each group of not more than ten samples, and at the end of the analytical run. All AOI were within the acceptance criteria of 90% to 110%.

Initial/Continuing Calibration Blank (ICB/CCB):

The ICB/CCB solution (5% v/v HNO₃) was analyzed immediately after the ICV solutions and after the CCV solutions (after each group of not more than ten samples and at the end of the analytical run). Sodium (Na) failed on ICP03.0-5 rerun and on the ICP03.0-6 rerun. These two were ran towards the end of the run where the higher concentration of acid digestion was run, which may lead to high concentrations of Na carrying over to the blanks. The ppm concentrations were 0.16 and 0.08 which are slightly above the EQL.

Low-Level Standard (LLS):

The LLS solution was analyzed immediately after the first CCB solution. All AOI were within the acceptance criteria of 70% to 130%.

Interference Check Standard (ICS/SST):

The ICS solution was analyzed immediately after the first LLS solution and immediately prior to analyzing the final CCV solutions. Recovery values are listed for all analytes included in the SST that were measured at or above the EQL. All AOI were within the acceptance criteria of 80% to 120%.

Serial Dilution (SD):

Five-fold serial dilution was conducted on sample 23-0331. The percent difference (%D) for all AOI were within the acceptance criteria of ≤ 10%.

Post-Digestion Spike (PS-A) - Sample (A Component):

A post-digestion spike (A Component) was conducted on sample 23-0331. All AOI were within the acceptance criterion of 80% to 120%.

Post-Digestion Spike (PS-B) - Sample (B Component):

A post-digestion spike (B Component) was conducted. There were no AOI included in the spike B component.

Post-Digestion Spike (PS-Q3A) - Sample (A Tormont Component):

Battelle PNNL/RPL/Inorganic Analysis ... ICP-OES Analysis Report

A post-digestion spike (A Tormont Component) was not conducted.

Post-Digestion Spike (PS-Q3B) - Sample (B Tormont Component):

A post-digestion spike (B Tormont Component) was not conducted.

Other QC:

All other instrument-related QC tests for the AOI passed within their respective acceptance criteria.

Comments:

- 1) The "Final Results" have been corrected for all laboratory dilutions performed on the samples during processing and analysis, unless specifically noted.
- 2) Instrument detection limits (IDL) and estimated quantitation limits (EQL) shown are for acidified water and/or fusion flux matrices as applicable. Method detection limits (MDL) for individual samples can be estimated by multiplying the IDL by the "Process Factor" for that individual sample. The estimated quantitation limit (EQL) for each concentration value can be obtained by multiplying the EQL by the "Process Factor".
- 3) Routine precision and bias is typically $\pm 15\%$ or better for samples in dilute, acidified water (e.g. 5% v/v HNO₃ or less) at analyte concentrations \geq EQL up to the upper calibration level. This also presumes that the total dissolved solids concentration in the sample is less than 5000 $\mu\text{g/mL}$ (0.5 per cent by weight). Note that bracketed values listed in the data report are within the MDL and the EQL, and have potential uncertainties greater than 15%. Concentration values $<$ MDL are listed as "-". Note, that calibration and QC standard samples are validated to a precision of $\pm 10\%$.
- 4) Analytes included in the spike A component (for the AS/PS) are; Ag, Al, As, B, Ba, Be, Bi, Ca, Cd, Co, Cr, Cu, Eu, Fe, K, Li, Mg, Mn, Mo, Na, Ni, P, Pb, Sb, Se, Si, Sm, Sn, Sr, Ta, Ti, Tl, V, W, Y, Zn, and Zr. Analytes included in the spike B component are; Ce, Dy, Eu, La, Nd, Pd, Rh, Ru, S, Te, Th, and U.

		Run Date >	3/23/2023	3/23/2023	3/23/2023	3/23/2023	3/23/2023	3/23/2023	3/23/2023	3/23/2023
		Process Factor >	1.0	1.0	421.7	421.7	356.8	1054.3	892.0	5271.3
			405 Diluent	23-0326 PB @1x	23-0331 @10x	23-0331 @10x Replicate	23-0331 Dup @10x	23-0331 @25x	23-0331 Dup @25x	23-0331 @125x SRD
Instr. Det. Limit (IDL)	Est. Quant. Limit (EQL)	Client ID >			1SY-23-COMP	1SY-23-COMP	1SY-23-COMP	1SY-23-COMP	1SY-23-COMP	1SY-23-COMP
(µg/mL)	(µg/mL)	(Analyte)	(µg/mL)	(µg/mL)	(µg/g)	(µg/g)	(µg/g)	(µg/g)	(µg/g)	(µg/g)
0.0019	0.019	Ag	--	--	--	--	--	--	--	--
0.0101	0.101	Al	--	--	3,350	3,370	2,630	3,340	3,290	3,270
0.0619	0.619	As	--	--	--	--	--	--	--	--
0.0060	0.060	B	[0.038]	[0.033]	[17]	[18]	[11]	[26]	[22]	[150]
0.0001	0.001	Ba	--	0.0078	[0.50]	[0.45]	[0.18]	[0.56]	[0.28]	--
0.0001	0.001	Be	--	--	--	--	--	--	--	--
0.0245	0.245	Bi	--	--	--	--	--	--	--	--
0.0056	0.056	Ca	--	[0.038]	[4.7]	[6.4]	[4.3]	[12]	[20]	[38]
0.0014	0.014	Cd	--	[0.0015]	--	[0.70]	--	--	--	[9.7]
0.0103	0.103	Ce	--	--	--	--	--	--	--	--
0.0043	0.043	Co	--	--	--	--	--	--	--	--
0.0020	0.020	Cr	--	--	97.5	97.9	75.7	99.1	96.3	[100]
0.0023	0.023	Cu	--	--	[2.8]	[2.6]	[1.9]	[2.6]	[3.4]	--
0.0023	0.023	Dy	--	--	--	--	--	--	--	--
0.0006	0.006	Eu	--	--	--	--	--	--	--	--
0.0014	0.014	Fe	--	0.0373	[1.0]	[1.9]	[0.90]	[2.2]	[8.0]	--
0.0312	0.312	K	[0.041]	--	293	282	316	369	327	[530]
0.0019	0.019	La	--	--	--	--	--	--	--	--
0.0007	0.007	Li	--	--	--	--	--	--	--	--
0.0018	0.018	Mg	--	[0.0029]	[0.87]	--	--	--	--	--
0.0002	0.002	Mn	--	--	[0.37]	[0.40]	[0.25]	[0.23]	[0.45]	--
0.0044	0.044	Mo	--	--	[9.4]	[10]	[8.5]	[16]	[11]	[52]
0.0073	0.073	Na	[0.010]	[0.031]	57,500	58,000	45,100	58,400	57,300	59,500
0.0088	0.088	Nd	--	--	--	--	--	--	--	--
0.0022	0.022	Ni	--	[0.0033]	[2.6]	[2.1]	[1.8]	--	[4.1]	--
0.0905	0.905	P	--	--	2,320	2,310	1,760	2,310	2,300	[2,700]
0.0269	0.269	Pb	--	--	--	--	--	--	--	--
0.0054	0.054	Pd	--	--	--	--	--	--	--	--
0.0211	0.211	Rh	--	--	--	--	--	--	--	--
0.0063	0.063	Ru	--	--	--	--	--	--	--	--
0.1262	1.262	S	--	--	650	654	486	[590]	[630]	[1,100]
0.0598	0.598	Sb	--	--	--	--	--	--	--	--
0.1656	1.656	Se	--	--	--	--	--	--	--	--
0.0086	0.086	Si	[0.022]	[0.013]	[4.4]	--	[4.8]	[23]	[16]	[100]
0.0291	0.291	Sn	--	--	--	--	--	--	--	--
0.0001	0.001	Sr	--	[0.0004]	[0.069]	[0.057]	[0.051]	[0.12]	--	--
0.0246	0.246	Ta	--	--	--	--	--	--	--	--
0.0197	0.197	Te	--	--	--	--	--	--	--	--
0.0071	0.071	Th	--	--	--	--	--	--	--	--
0.0006	0.006	Ti	--	[0.0008]	--	--	--	--	--	[3.7]
0.0814	0.814	Tl	--	--	--	--	--	--	--	--
0.0410	0.410	U	--	[0.042]	[19]	--	[16]	--	[59]	[300]
0.0013	0.013	V	[0.0028]	[0.0031]	[2.9]	[2.9]	[2.5]	[4.9]	[4.1]	[13]
0.0161	0.161	W	--	--	--	[6.8]	--	--	--	--
0.0006	0.006	Y	--	--	--	--	--	--	--	--
0.0027	0.027	Zn	--	[0.019]	[2.3]	[2.0]	--	--	--	--
0.0014	0.014	Zr	--	--	--	--	--	--	--	--

1) "--" indicates the value is < MDL. The method detection limit (MDL) = IDL times the "multiplier" near the top of each column. The estimated sample quantitation limit = EQL (in Column 2) times the "multiplier". Overall error for values ≥ EQL is estimated to be within ±15%.

2) Values in brackets [] are ≥ MDL but < EQL, with errors likely to exceed 15%.

na = not applicable; KOH flux and Ni crucible or Na₂O₂ flux and Zr crucible for fusion preparations, or Si for HF assisted digests.

		Run Date >	3/23/2023	3/23/2023
		Process Factor >	5271.3	4460.0
			23-0331 @125x SRD Rep.	23-0331 Dup @125x SRD
Instr. Det. Limit (IDL)	Est. Quant. Limit (EQL)	Client ID >	1SY-23-COMP	1SY-23-COMP
(µg/mL)	(µg/mL)	(Analyte)	(µg/g)	(µg/g)
0.0019	0.019	Ag	--	--
0.0101	0.101	Al	3,320	3,330
0.0619	0.619	As	--	--
0.0060	0.060	B	[110]	[65]
0.0001	0.001	Ba	[1.1]	--
0.0001	0.001	Be	--	--
0.0245	0.245	Bi	--	--
0.0056	0.056	Ca	[54]	[64]
0.0014	0.014	Cd	--	--
0.0103	0.103	Ce	--	--
0.0043	0.043	Co	--	--
0.0020	0.020	Cr	107	101
0.0023	0.023	Cu	--	--
0.0023	0.023	Dy	--	--
0.0006	0.006	Eu	--	--
0.0014	0.014	Fe	--	--
0.0312	0.312	K	[540]	[480]
0.0019	0.019	La	--	--
0.0007	0.007	Li	--	--
0.0018	0.018	Mg	--	[11]
0.0002	0.002	Mn	--	--
0.0044	0.044	Mo	--	[29]
0.0073	0.073	Na	59,900	57,900
0.0088	0.088	Nd	--	--
0.0022	0.022	Ni	--	[14]
0.0905	0.905	P	[2,100]	[2,400]
0.0269	0.269	Pb	--	--
0.0054	0.054	Pd	--	--
0.0211	0.211	Rh	--	--
0.0063	0.063	Ru	--	--
0.1262	1.262	S	[780]	--
0.0598	0.598	Sb	--	--
0.1656	1.656	Se	--	--
0.0086	0.086	Si	[60]	[63]
0.0291	0.291	Sn	--	--
0.0001	0.001	Sr	--	--
0.0246	0.246	Ta	--	--
0.0197	0.197	Te	[160]	[120]
0.0071	0.071	Th	--	--
0.0006	0.006	Ti	--	--
0.0814	0.814	Tl	--	--
0.0410	0.410	U	--	--
0.0013	0.013	V	[16]	[14]
0.0161	0.161	W	--	--
0.0006	0.006	Y	--	--
0.0027	0.027	Zn	--	--
0.0014	0.014	Zr	--	--

1) "--" indicates the value is < MDL. The method detection limit (MDL) = IDL times the "multiplier" near the top of each column. The estimated sample quantitation limit = EQL (in Column 2) times the "multiplier". Overall error for values ≥ EQL is estimated to be within ±15%.

2) Values in brackets [] are ≥ MDL but < EQL, with errors likely to exceed 15%.

na = not applicable; KOH flux and Ni crucible or Na₂O₂ flux and Zr crucible for fusion preparations, or Si for HF assisted digests.

Appendix E – Backpulsed Solids from SY-101 Characterization with Scanning Transmission Electron Microscopy

Materials from a concentrate from Hanford tank waste material representing tank 241-SY-101 (herein SY-101) were run through the backpulse dead-end filter (BDEF) system at 16 °C. These concentrates were examined with scanning electron microscopy (SEM), scanning transmission electron microscopy (STEM) with X-ray energy dispersive spectroscopy (EDS), and transmission electron microscopy (TEM) with selected area electron diffraction (SAED) in the Radiochemical Processing Laboratory (RPL) at Pacific Northwest National Laboratory. The sample was received as a liquid with suspended solids that had been centrifuged to concentrate the solids. Samples for microscopy analyses were prepared using a filtering method to avoid the formation of evaporative salts to the best extent possible. The solutions were wicked through a lacey carbon support a TEM grid made of copper. The samples were examined by SEM to image the largest particles and then in the STEM/TEM instrument. Large particles were manually removed from the TEM grid as these could not be examined in this instrument if the particles were larger than 20 to 50 μm , and presented an unnecessary contamination hazard.

The SEM instrument used was an FEI (Thermo-Fisher Inc., Hillsboro, OR) equipped with backscattered electron detector and a transmission STEM detector. During this analysis, the EDS system on the tool was unavailable. The magnification scale was checked against an MRS-4 standard. The STEM/TEM instrument used was a JEOL (JEOL Inc., Japan) ARM300F (GrandARM) microscope. STEM images were collected using a high-angle annular dark-field (HAADF) detector and compositional analysis was obtained with EDS. Samples were also imaged with TEM, high-resolution TEM (HRTEM), and SAED. Diffraction patterns were analyzed with CrysTBox (Crystallographic Tool Box) software (Klinger 2017). Particle analysis was performed using Python scripts in a Jupyter notebook.

E.1 Microscopy Solids Analysis Results

Large particles, over 200 μm diameter, were observed frequently; however, it was not possible to analyze these in the STEM microscope. With SEM, the very large particles could be easily accommodated, but the STEM/TEM analysis is limited to particles less than 10 μm in diameter. Indeed, unless the particles are more than 30 nm thick, it is not possible to get good quality STEM/TEM analysis. The large particles had to be physically removed from the TEM grid prior to introduction in the TEM chamber. Large particles could also result in unnecessary contamination and potential damage to the instrument.

E.1.1 SY-101 Solids

The agglomerated multiphase material shown in Figure E.1 was commonly found throughout the sample. This specific particle agglomerate was found to consist mainly of Al, Na, Mg, Si, Fe, Ca, and O. Carbon was present in the support film, but it was usually possible to distinguish this signal from the carbon in a phase. Copper X-ray fluorescence from the grid resulted in the production of Cu K- and L- lines, and these were observed in all the analyses. Figure E.2 shows STEM-HAADF and STEM EDS maps from the yellow box highlighted area from Figure E.1. In Figure E.2, there is evidence of an Al-Cr phase that was commonly observed together with a discrete Ca-rich region. Further analysis showed that the calcium phase was a calcium phosphate phase, apatite, in most instances. Figure E.3 (A-C) shows three different phases observed in an agglomerated particle. SAED in TEM mode was used to obtain structural information on the different phases. The three phases appeared to be an aluminosilicate, a layered silicate, and a calcium phase, calcite. The electron diffraction is listed in Table E.1.

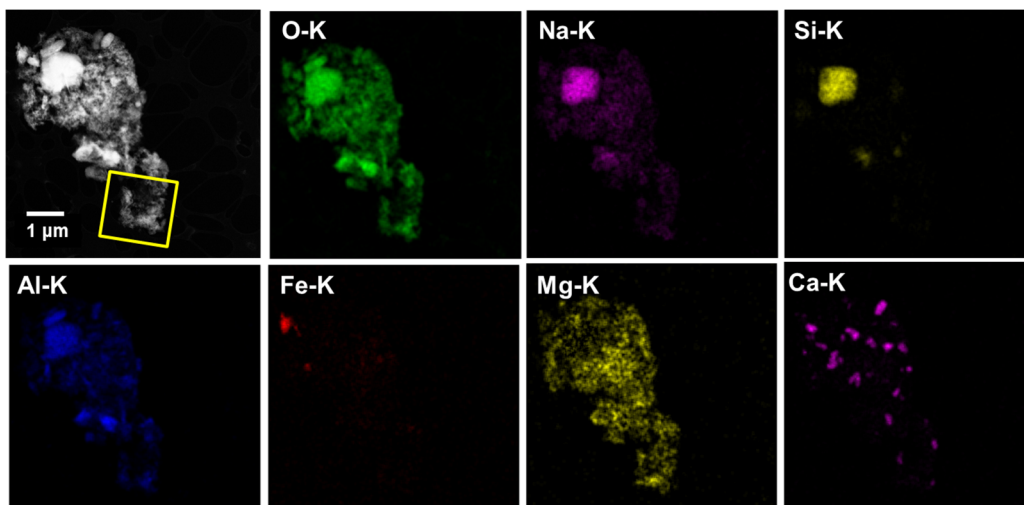


Figure E.1. STEM image of a large agglomerate and STEM-EDS maps of SY-101.

Table E.1. Electron diffraction from calcite particle and Al-silicate particle.

d-spacing [nm]			d-spacing [nm]		
Plane	theor. calcite	measured	Plane	theor. kaolinite	measured
(0 2 2)	0.209	0.217	(0 2 0)	0.446	0.500
(1 1 6)	0.188	0.181	(1 1 2)	0.352	0.354
(1 2 1)	0.163	0.161	(0 2 4)	0.279	0.279
(1 2 4)	0.153	0.153	(1 3 1)	0.249	0.250
(1 2 7)	0.136	0.137	(1 1 5)	0.225	0.225
(0 3 6)	0.129	0.131	(0 4 4)	0.189	0.190
(1 3 2)	0.119	0.117	(1 1 7)	0.175	0.173
(2 2 6)	0.114	0.115	(3 1 4)	0.141	0.141
(2 3 4)	0.097	0.097	(7 3 4)	0.067	0.067

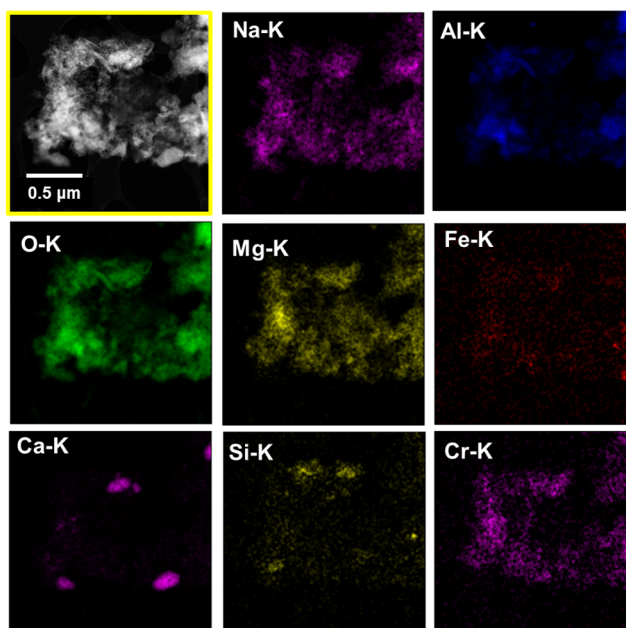


Figure E.2. Further STEM-EDS maps from the yellow-marked out region from Figure E.1 from the SY-101 agglomerated material.

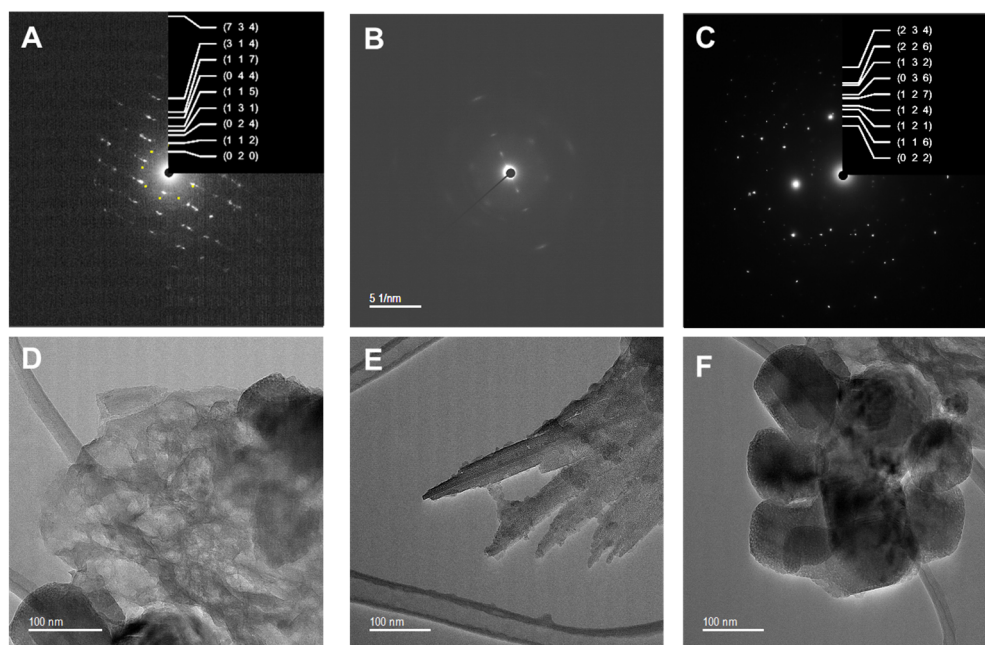


Figure E.3. TEM/SAED analysis of three different phases (A) Al-silicate, (B) layered silicate phase, and (C) calcite.¹

¹ Ref: (A) Diff003 80cm SY-101 0268.dm4, (B) Diff005 80cm SY-101 0271.dm4, (C) Diff007 80cm SY-101 0269.dm4

The diffraction pattern shown in Figure E.3A was analyzed with CrysTBox software (Klinger 2017) using potential matches from the American Mineralogist Crystallographic Database (<http://rruff.geo.arizona.edu/AMS/amcsd.php>) for kaolinite. Kaolinite was used because the Al:Si ratio was close to 1.0. The phase identified in Figure E.3C was thought to be calcite as only Ca and O were detected. It is thought that calcium originates from the process water and is nucleated from reaction with ligands that were present in the supernate. Calcite (CaCO_3) is a major carbonate mineral that is known to occur in the Hanford tanks (see Figure E.3); however, most of the other calcium phases found in SY-101 were apatite. Calcite phases might also incorporate Mg^{2+} and Al^{3+} . However, STEM-EDS did not indicate the presence of Al in this phase.

The occurrence of an amorphous chromium aluminum hydroxide coprecipitate has long been considered in the Hanford tanks (Fiskum et al. 2008) Chatterjee et al. (2016) considered the possibility that Cr could be incorporated into boehmite, a dominant Al-oxide observed in the tank wastes, and its impact on the dissolution of this phase. An EDS analysis of a Cr-bearing Al-phase is shown in Figure E.4. Figure E.5 and Figure E.6 show further analyses of these Cr-containing Al-phases. TEM images show a whispery nature to this phase. STEM-HAADF images and STEM-EDS elemental maps of the material revealed the composition.

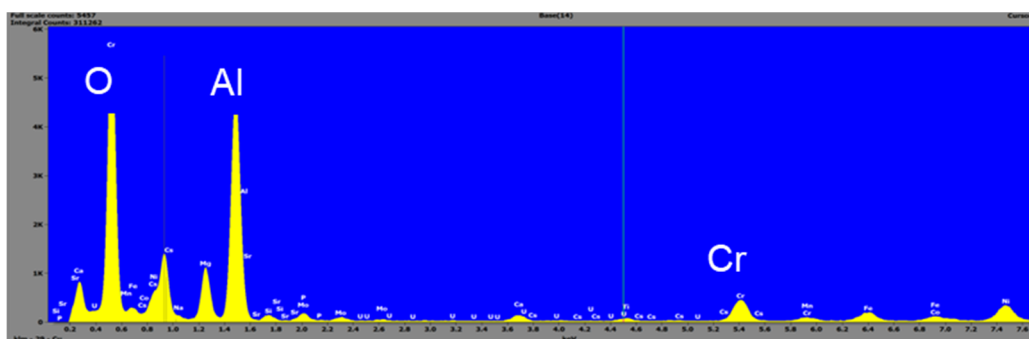


Figure E.4. TEM-EDS of Al-phase shown in Figure 4.11 indicating the presence of Cr in the phase.

The TEM images in Figure E.5 show an aluminum oxide particle agglomerate from the SY-101 sample together with a weak SAED pattern, and an HRTEM image with an insert fast Fourier transform (FFT) diffraction pattern. Note that the speckled pattern in the TEM image indicates nano-features.

In Figure E.5A, there are several other dominant phases present, including a calcium phase that was previously identified as an apatite-type mineral phase. Some of the EDS analyses here suggested the presence of fluorine in these phases, which would indicate that these were hydroxy-fluoro-apatites. The feature of interest in this analysis was the Al-Cr phase (indicated by the yellow box to the far right of the image). The Cr level was relatively small but was consistently in the phase according to the STEM-EDS maps. HRTEM imaging was performed on the phase shown in Figure E.5B. These images indicated that the phase was composed of nanocrystalline particles. This might indicate a particle attachment process that was occurring in the formation of the material, which may be causing the nano-features that were found in Figure E.5. More definitive electron diffraction is shown in Figure 4.11 with the comparison with boehmite. This phase remains elusive but the composition and morphology were consistent. Further analysis of this phase is needed to determine the exact nature of the phase.

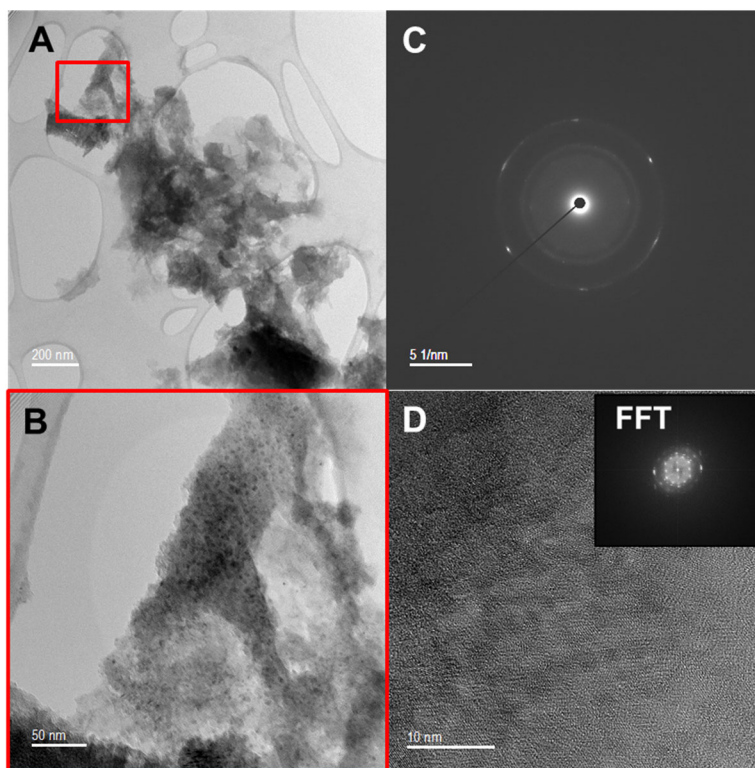


Figure E.5. (A-B) TEM images of an aluminum oxide particle agglomerates from the SY-101 sample (C) SAED pattern, and (D) HRTEM and insert FFT diffraction pattern.

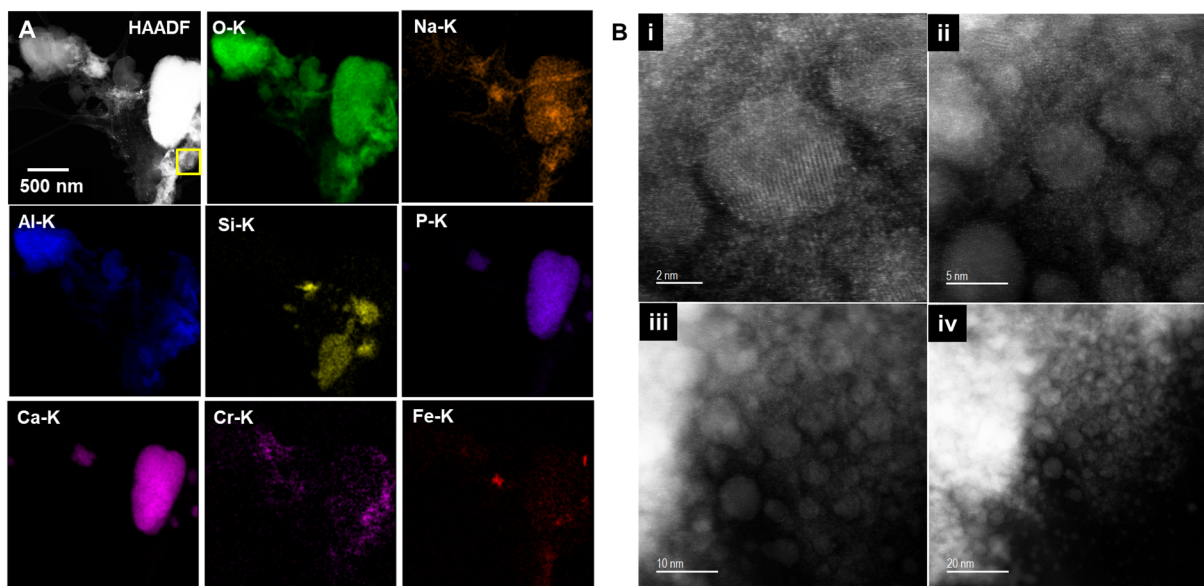


Figure E.6. (A) HAADF image and STEM-EDS maps of SY-101 showing a calcium phosphate and an Al-Cr phase and (B) HRTEM images, decreasing in magnification (i to iv) of yellow-boxed region in (A) from Al-Cr phase showing nanocrystalline nature of this region.

Figure E.7 and Figure E.8 show a series of aluminum oxide particles that were previously identified as gibbsite and calcium phosphates, identified as an apatite-type phase. These were common in the sample. The Mg and Cr signals did appear overlap with Al, indicating that there is also a common phase within the agglomerate. The quantity of Al was high throughout the specimen, so in some phases such as this one where it did not seem high, there is still significant Al present. The arrangement of different phases in the agglomerated particles was complex. In Figure E.8, iron particles and a molybdenum particle were found. These elemental maps were analyzed with a principal component analysis method to reveal the individual phase compositions, and this is shown in Figure E.9.

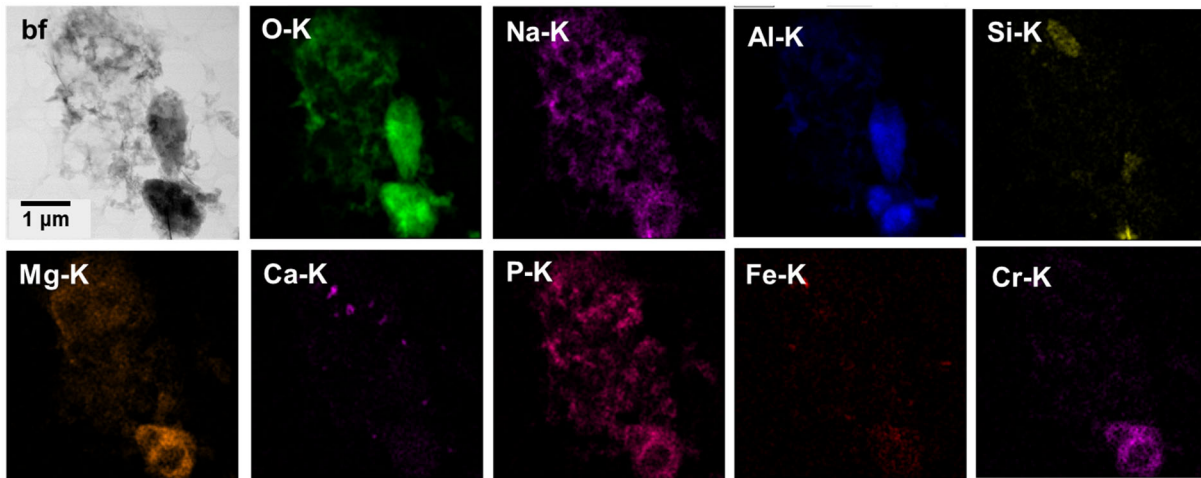


Figure E.7. Bright-field STEM image and STEM-EDS maps of SY-101 with Al-oxide, as well as phosphate, magnesium, and chromium bearing phases.

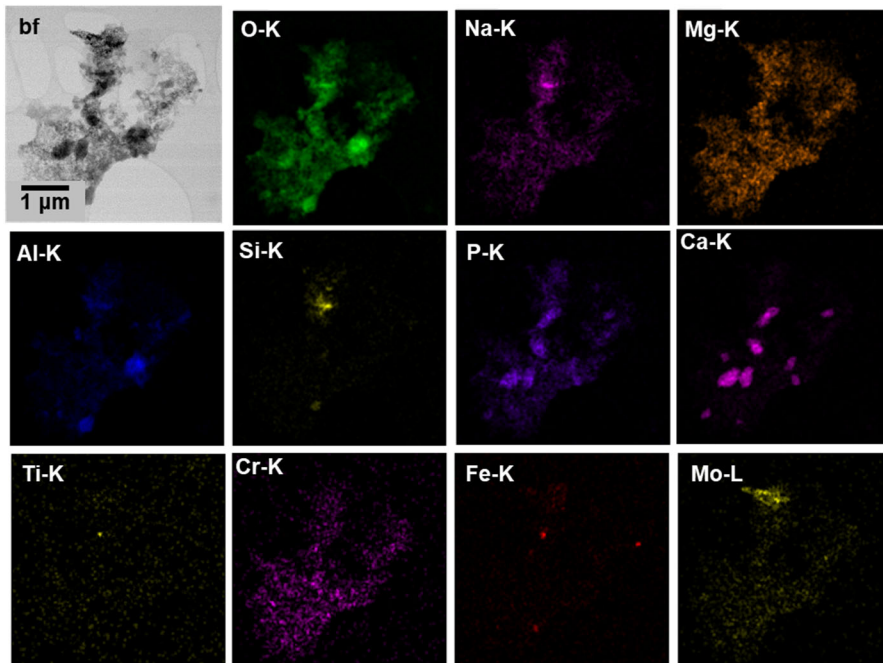


Figure E.8. STEM-b.f. image and SEM-EDS elemental maps of SY-101 showing the apatite, gibbsite, iron, Al-Cr phase, sodium silicate, and Mo-rich phase.

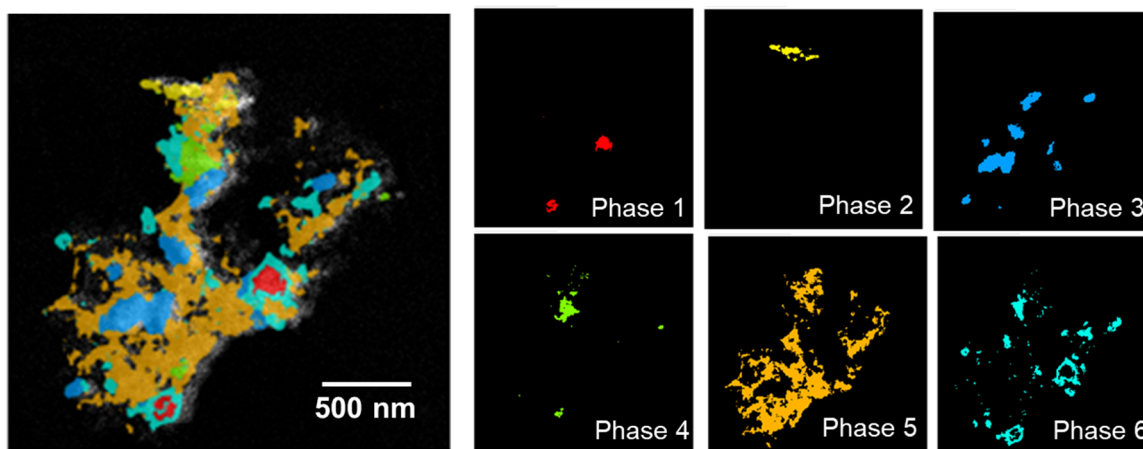


Figure E.9. Phase analysis of SY-101 using principal component analysis. Phase 1 was the Al-oxide (gibbsite), Phase 2 was the Mo-phase, Phase 3 was the calcium phosphate (apatite), Phase 4 was the Na-silicate, Phase 5 was the Al-Cr phase, which may also contain Mg.

Particle size analysis was performed on the particles from the TEM grids in the SEM. The resulting distribution is shown in Figure E.10.

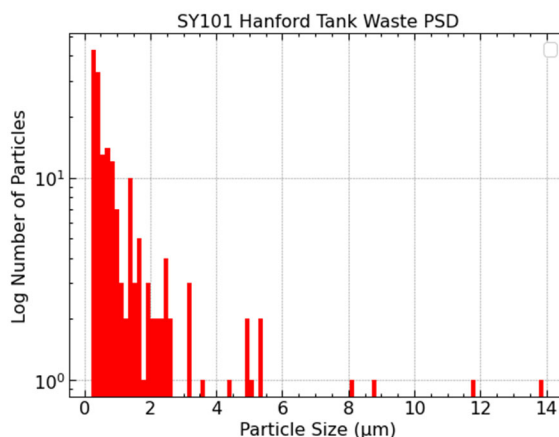


Figure E.10. Particle size distribution from particles observed on the TEM grids (note that many of the particles observed were far larger).

E.2 Conclusions of Microscopy Study

The study only used STEM and TEM methods to analyze collected solids. A few different compositions were found, including aluminum oxide (gibbsite), calcium phosphate (apatite), calcium carbonate (calcite), Al-Cr-phase, iron particles, and alumino-silicates. Electron diffraction was able to identify gibbsite and apatite clearly. Other phases were difficult to distinguish.

E.3 References

Chatterjee S, M Conroy, F Smith, H-J Jung, Z Wang, RA Peterson, A Huq, DG Burtt, ES Ilton, and EC Buck. 2016. "Can Cr(III) substitute for Al(III) in the structure of Boehmite?" *RSC Advances*.
<https://doi.org/doi:10.1039/C6RA20234A>

Fiskum SK, EC Buck, RC Daniel, KE Draper, MK Edwards, TL Hubler, LK Jagoda, ED Jenson, AE Kozelisky, and GJ Lumetta. 2008. *Characterization and Leach Testing for REDOX Sludge and S-Saltcake Actual Waste Sample Composites*. PNNL-17368, Pacific Northwest National Laboratory, Richland, WA.

Klinger M. 2017. "More features, more tools, more CrysTBox." *Journal of Applied Crystallography* 50(4):1226-1234. <https://doi.org/doi:10.1107/S1600576717006793>

Pacific Northwest National Laboratory

902 Battelle Boulevard
P.O. Box 999
Richland, WA 99354
1-888-375-PNNL (7665)

www.pnnl.gov